Canadian Science Publishing | Canadian Geotechnical Journal

Effects of sampling disturbance in geotechnical design

Journal:	*Canadian Geotechnical Journal*
Manuscript ID	cgj-2018-0016.R1
Manuscript Type:	Article
Date Submitted by the Author:	19-May-2018
Complete List of Authors:	Lim, Guan Tor; The University of Western Australia, Centre for Offshore Foundations Systems Pineda, Jubert; The University of Newcastle, ARC Centre of Excellence for Geotechnical Sciences and Engineering Boukpeti, Nathalie; The University of Western Australia, Centre for offshore foundation systems Carraro, J. Antonio H.; Imperial College London, Department of Civil and Environmental Engineering Fourie, Andy; The University of Western Australia, School of Civil and Resource Engineering
Keyword:	soil disturbance, soft clay, tube sampling, geotechnical design
Is the invited manuscript for consideration in a Special Issue? :	Not applicable (regular submission)

17 May 2018

Effects of sampling disturbance in geotechnical design

Guan Tor Lim[1], Jubert Pineda[2] , Nathalie Boukpeti [1], J. Antonio H. Carraro[3] and Andy Fourie[4]

[1] Centre for Offshore Foundation Systems, The University of Western Australia, Perth, WA, Australia

[2] ARC Centre of Excellence for Geotechnical Science and Engineering, The University of Newcastle, Newcastle, NSW, Australia

[3] Department of Civil and Environmental Engineering,
Imperial College London (formerly at COFS),

[4]School of Civil, Environmental and Mining Engineering
The University of Western Australia

Keywords: sample disturbance, soft clay, stiffness, compressibility, strength, geotechnical design

ABSTRACT

This paper describes an experimental study of the effects of sampling disturbance in an Australian natural soft clay and the consequences of different sample quality on the representativeness of soil parameters used in geotechnical designs. The paper is divided into three sections. Laboratory test results obtained from specimens retrieved using three different tube samplers as well as the Sherbrooke (block) sampler are first described. Then, the sample quality assessment, using available indices proposed for soft soils, is presented. It is shown that sample quality varies with the stress paths and boundary conditions applied in laboratory tests. Finally, mechanical soil properties derived from specimens retrieved using the different samplers are used in the prediction of two classical problems in soil mechanics: the settlement and excess pore pressure response underneath an embankment as well as the settlement and bearing capacity of a

shallow footing. These two examples are used here to highlight the consequences of poor sampling in practice.

1 INTRODUCTION

The Embankment Prediction Symposium (CGSE 2016), recently organized in Newcastle (NSW, Australia) by the ARC Centre of Excellence for Geotechnical Science and Engineering (CGSE), aimedto predict the behaviour of an embankment built on natural soft clay improved with vertical drains (PVDs) from the Ballina field testing facility, located in northern NSW. Results of detailed *in situ* and laboratory characterization studies (Pineda et al. 2016a; Kelly et al. 2017) were provided to Australian and international predictors, including practitioners and academics. The laboratory study was carried out on tube specimens retrieved using a fixed piston sampler (89 mm diameter), which provided soil specimens of *excellent* as well as *good to fair* quality according to available sample quality indexes for soft clays (Lunne et al. 1997).

The fixed piston sampler was preferred instead of other sampling techniques (including block sampling) for two main reasons. First, block sampling is a cost-prohibitive technique almost never used in common practice. Second, fixed piston samplers are known for providing specimens of better quality compared with other tube sampling techniques such as open samplers (Shelby tubes) and free piston samplers (e.g., Andersen and Kolstand 1979; Lacasse et al. 1985; Tanaka et al. 1996; Lunne et al. 1997; Ladd and DeGroot 2003; Lunne et al. 2006; Landon et al. 2007; Donohue and Long 2010; Pineda et al. 2016b; to name a few). Despite their well-documented advantages, the use of fixed piston samplers is still not well established in practice. In Australia, for instance, Shelby tubes (50 – 75 mm in diameter) are the typical choices, mainly due to their simple operational principle. However, mechanical parameters obtained from laboratory tests performed on Shelby tubes in most cases do not represent the *in situ* conditions. Laboratory testing is expensive and involves long testing times, so additional sampling and laboratory campaigns tend to be avoided in practice, even if the quality of soil specimens does not fulfil the recommendations given in the literature. Therefore, there is a concern about the influence of soil disturbance as a result of sampling on predicted soil behaviour for typical geotechnical infrastructure.

For this study, samples were obtained from the same depth at the Ballina field testing facility using four different samplers in order to assess the level of sample disturbance and its effect on the mechanical parameters of natural Ballina clay. In addition, the consequences of the sampling disturbance on the predicted settlement and excess pore pressure underneath an embankment as well as the predicted settlement and bearing capacity of a shallow footing are presented. These two classical problems provide a good benchmark exercise for the quantification of the error(s) caused by poor sampling in geotechnical design.

2 TESTED SOIL AND SAMPLING PROGRAM

Ballina clay is a structured and lightly overconsolidated (OCR<2) marine clay (Holocene age) encountered at the Ballina field testing facility, in northern New South Wales (Australia). Ballina clay is

mainly composed of kaolinite,illite, quartz, illite-smectite and amorphous minerals. It has an activity of 1.0 and a plasticity index that ranges between 30% and 85% (i.e., high to extremely high plasticity). Site characterization studies (Pineda et al. 2016; Kelly et al. 2017) divided the soil profile at Ballina site into four main layers (see Figure 1). Layer 1 corresponds to a sandy clayey silt alluvial crust (~ 1.5 m thick). Layer 2 is the upper estuarine silty clay strata (~ 2.5 m thick) for which plasticity and void ratio increases (dry density decreases). Layer 3 corresponds to a lower estuarine silty clay layer (~ 7 m thick) with nearly constant soil properties which overlies a 4 m thick clayey silty sand transition layer (Layer 4). As observed in Figure 1, the *in situ* water content and dry density vary with depth from 20% to 120% and between 1.50 and 0.70 Mg/m^3, respectively. The soft clay layer encountered between 2 m and 11 m depth has a predominant clay fraction with maximum values up to 82 %. A non-oriented fabric was distinguished using scanning electron microscopy analysis (SEM), which is consistent with its low permeability anisotropy (see Kelly et al. 2017).

Figure 1. Variation of index properties with depth at the Ballina field testing facility (modified from Pineda et al. 2016a)

Specimens tested in this study were obtained using three different tube samplers as well as the Sherbrooke (block) sampler (Lefebvre and Poulin 1979). Figure 2 shows the plan view of the Ballina testing facility including the location of the boreholes (drilled using mounted rigs) which corresponds to the distribution of the instrumentation used for monitoring the performance of two embankments, named as PVD and No PVD. Also included in this figure are the location of the seismic flat dilatometer test SDMT-8, cone penetration (CPTu) and field vane (FV) tests, which are used in the analysis described below. Samples were retrieved from a depth of 5.5 - 6.1 m as indicated in Figure 1. The U75 Shelby tube (75 mm diameter) was used in borehole *Inclo 4* whereas the free piston sampler P100 (100 mm diameter) was employed in borehole *Inclo 1*. The O89 fixed-piston sampler (89 mm diameter) was the choice in borehole *Standpipe*. Finally, a block specimen was retrieved fromborehole *BH1* using the Sherbrooke sampler (250 mm diameter) which has been recognized to provide the highest sample quality in soft clays (e.g., Hight et al. 1992; Lunne et al. 1997; Lunne et al. 2006). The dimensions and characteristics of the tube samplers are summarized in Table 1. A schematic view is given in Figure 3. All samplers have an area ratio (AR) lower than 14 % which is less than a typical thick-walled composite piston sampler. The ratio between external diameter and thickness of the tube wall (D_e/t) varies between 33.3 (P100) to 50.7 (U75). The outer cutting angle (OCA) for the U75 and O89 tubes is 15^o and 5^o, respectively. The OCA for the P100 tube is 90^o as it represents the standard version available in the market. It can be noted that according to the suggestions for tube sampling given by Ladd and De Groot (2003) ($D_e/t > 40$; OCA < 10^o and AR< 10%), the U75 sampler should provide (a priori) the highest sample quality whereas the lowest quality should be obtained with the P100 free-piston sampler. After sampler retrieval, tube ends were properly sealed in-situ with several layers of plastic film underlying a 10mm-thick polystyrene (porexpan) plate covered externally with wax (10-15mm thickness). The porexpan plate was intended to isolate the clay from the thermal gradient. Silicone grease was applied at the interfaces between the tube sampler and the porexpan plate for improving sealing. Tube ends were finally covered with plastic lids prior to packing for transport. The block specimen was sealed using several layers of plastic film and

aluminium foil prior to waxing. Specimens were placed in sealed plastic containers on a layer of wet sand aimed at minimizing moisture losses by creating a high relative humidity environment (RH= 99 %). The tubes and the block were packed using scraps of polystyrene beads to induce lateral confinement and to absorb vibrations during transport.

Table 1: Dimensions of the samplers used in this study

Figure 2. Location of the boreholes at the Ballina field testing facility

Figure 3. Samplers used in this study. (a) Shelby tube (from Clayton et al. 1995). (b) Free piston sampler. (c) Fixed-piston sampler (from ASTM D6519-08). (d) Sherbrooke (block) sampler.

3 EXPERIMENTAL PROGRAM AND LABORATORY PROCEDURES

Bender elements (BE) tests (for wave propagation assessment), resonant column (RC) tests, one-dimensional constant rate of strain (CRS) compression tests and simple shear (SS) tests with cell pressure confinement were carried out in this study to evaluate the stiffness, compressibility and strength parameters, respectively, of Ballina clay specimens. The allocation of specimens is indicated in Figure 4. Tube samples were sliced horizontally before trimming to minimize the adhesion force at the clay-tube interface during specimen extrusion. A brief description of each of the testing procedures is given in the following sections.

Figure 4: Specimen allocation in a tube (U75, P100 and O89 tube specimens) and block samples.

3.1 Bender element tests

Shear wave velocity was evaluated on the sectioned tube slices later used for one-dimensional CRS compression tests, before and after soil extrusion, using BE transducers manufactured at The University of Western Australia (UWA). A sine pulse of peak to peak voltage, V_{pp} of 20 V with apparent frequency f_{app} = 5 kHz was used as input signal. The effective length, l_{eff}, was determined as the tip-to-tip distance between the piezoceramic elements. The travel time, t_s, was estimated as the time interval between the first peak of the transmitted and received signal. The testing procedure followed the protocol described in Viggiani and Atkinson (1995). The shear wave velocity was estimated as $V_{s(ij)}= l_{eff}/t_s$, where subscripts *i* and *j* refer to the wave propagation and polarization directions, respectively.

3.2 Resonant column tests

A Stokoe fixed-free type of resonant column apparatus (GDS Instruments Ltd., UK) was used to assess the small-strain shear modulus, $G_{(vh)}$, as well as the damping ratio, D, of Ballina clayspecimens. The apparatus is similar to that described in Clayton (2011) and was designed to minimize equipment damping. The RC tests were controlled via software using GDSLAB and GDSRCA packages.

Specimens tested were 140 mm in height and 72 mm in diameter. Specimens were saturated under

5 kPa isotropic effective stress by applying a back pressure of 500 kPa in stages. Low isotropic effective stress was used to prevent over stressing the specimen during saturation. Values of Skempton's B parameter higher than 0.96 were measured in all specimens after 1.5 days of saturation under the back pressure of 500 kPa. Specimens were then isotropically consolidated to an *in situ* mean effective stress $p'_{in\ situ} = (\sigma¢_v + 2\sigma¢_h) / 3 = 31$ kPa, based on estimated vertical and horizontal *in situ* effective stresses ($\sigma¢_{v\text{-}in\ situ} = 42$ kPa and $\sigma¢_{h\text{-}in\ situ} = 25.2$ kPa, for $K_0 = 0.60$) according to Kelly et al. (2017). Consolidation stress increments were applied in 5 kPa increments.

The RC testing procedure followed the recommendations outlined by ASTM Standard D4015 (2007). A sinusoidal torsional vibration was applied to the top of the specimen to allow propagation of shear waves. The shear wave velocity measured in vertical direction, $V_{s(v)}$, was estimated as:

$$V_{s(v)} = \frac{2\pi f l}{\beta} \tag{1}$$

where f is the torsional resonant frequency, l is the length of the specimen and β is the device's calibration factor which accounts for the mass moment of inertia of the specimen as well as the mass moment of inertia of the components mounted on the specimen (i.e., drive system, accelerometer, top platen and counterweight masses). The damping ratio, D was estimated from the logarithmic decrement of free vibration decay curve, δ, accordingto:

$$D = \sqrt{\frac{\delta^2}{4\pi^2 + \delta^2}} \tag{2}$$

3.3 One-dimensional constant rate of strain compression tests

CRS tests were carried out to evaluate the compressive behaviour of Ballina clay. CRS tests followed the recommendations given by ASTM D4186 (2006). Cylindrical specimens (50 mm in diameter and 24 mm in height) were tested using a Trautwein cell in combination with a computer-controlled loading frame. Specimens were saturated for 48 hours under a vertical effective stress of 10 kPa. Then, the vertical load was applied under a constant strain rate of 1.0 %/h until a maximum vertical effective stress of 500 kPa was reached. Single drainage was allowed during compression while the excess pore water pressure was measured at the specimen base. The adopted strain rate produced excess pore water pressures lower than 20 % of the total vertical stress in all tests except for one test when a maximum value of 30 % was reached.

3.4 Simple shear tests with cell pressure confinement

Undrained monotonic simple shear tests with cell pressure confinement were performed to estimate the undrained shear strength of Ballina clay specimens. These SS tests were carried out in the UWA simple shear apparatus similar to that described by Mao and Fahey (2003). In this apparatus, specimens with dimension and height equal to 72 and 40 mm respectively were enclosed in an unreinforced latex membrane. During the shearing phase, the total vertical stress was kept constant by varying the cell

pressure via software and the sample height was maintained constant by mechanically locking the vertical actuator.

The testing procedure included three stages: saturation, anisotropic consolidation and undrained shearing. A back pressure equal to 400 kPa was ramped during the saturation stage while maintaining a mean effective stress of 10 kPa on the specimen. Skempton's B parameter was higher than 0.98 in all tests after 1 day of saturation. Specimens were then consolidated to their *in situ* stress state defined by $\sigma¢_{axial}$ = 42 kPa and $\sigma¢_{radial}$ = 25.2 kPa, as discussed above. An equalization time of 24 h was allowed for all specimens after achieving the *in situ* stress state. Finally, shearing under undrained conditions was conducted using a horizontal strain rate of 2%/h, following the recommendations by ASTM D6528 (2007) using c_v determined from CRS tests.

4 RESULTS

4.1 Shear wave velocity

Figure 5 shows the shear wave velocity determined from block and tube specimens devoted to CRS testing. Vs with horizontal polarization was measured in both vertical ($Vs_{(vh)}$) and horizontal ($Vs_{(hh)}$) directions. In the case of tube specimens, vertical measurements were made before ($Vs_{(vh)\text{-tube}}$) and after specimen extrusion ($Vs_{(vh)\text{-extruded}}$). In both cases, BE transducers were carefully inserted 3 mm on top and bottom faces of each sample. The comparison against *in situ* values obtained from seismic flat dilatometer test SDMT-8 (Figure 5(a)) shows that $Vs_{(vh)}$ is more strongly affected by sampling than $Vs_{(hh)}$. The largest stress relief due to sampling, which takes place in the vertical direction, seems to be responsible for the highest reduction in $Vs_{(vh)}$. The fact that $Vs_{(hh)block} » Vs_{(vh)SDMT}$, supports the observation that stress relief due to sampling affects $Vs_{(vh)}$ more than $Vs_{(hh)}$. It is important to note that despite the sedimentary nature of the clay, which could explain the higher values of $Vs_{(hh)}$, scanning electron microscopy (SEM) analysis has shown a non-oriented fabric for natural Ballina clay. In fact, values of $Vs_{(vh)}$ similar to those obtained from SDMT have been measured in CRS tests at $s'_v = s'_{v\text{-}in\ situ}$ by Pineda et al. (2016a) on specimens obtained using a sampler similar to O89. Hence, *in situ* values obtained from SDMT can be used as good references as the results have shown consistent agreement with shear wave velocity from bender element measurement in the laboratory (Pineda et al. 2016a). Block and O89 specimens show the highest and second highest shear wave velocities respectively for both directions while the P100 and U75 samples show the lowest $Vs_{(vh)}$ and $Vs_{(hh)}$, respectively. Soil extrusion produces an additional reduction in Vs as indicated by $Vs_{(vh)\text{-extruded}}$. This is more evident in the case of the P100 sample. The Vs normalised by $Vs_{(vh)SDMT}$ is plotted in Figure 5(b) and shows that sampling causes a reduction in $Vs_{(vh)}$ between 21% for O89 and 31% for P100 free-piston sampler whereas in the case of $Vs_{(hh)}$ it decreases by 28% for U75 Shelby sampler.

Figure 5. **Variation of (a) shear wave velocity and (b) normalised shear wave velocity with sampler**

diameter

4.2 Small-strain stiffness

Figure 6 shows the variation of the small-strain shear modulus measured in the vertical direction, G_v, with the shear strain, γ, obtained from RC tests for block, P100 and U75 specimens. Poor coupling between the pedestal and the O89 specimen led to some erroneous measurements, which have therefore been omitted in Figure 5 for consistency. The RC test for the P100 specimen was stopped at γ=0.02%due to malfunctioning of the resonant column device. It caused a sudden jump in the resonant frequency that led to values of G_v around 2-3 times larger the ones measured for the block sample. Because of this unjustified response, only values of G_v below γ=0.02% are reported in Figure 6 for this specimen. Values of G_v, estimated from BE tests using the bulk density of CRS specimens, are included in Figure 6(a) for comparison. The comparison between BE and RC results shows an important increase in G_v due to sample recompression to $p¢_{in\text{-}situ}$ in the RC apparatus. Similar values to the *in situ* small-strain stiffness (SDMT-8) are reported for the block specimen whereas lower values are observed for specimens P100 and U75. This behaviour confirms the negative effect of tube sampling on soil fabric. For the same strain level, values of G_v in specimens P100 and U75 are approximately 1.5 MPa and 2.50 MPa lower than the block sample, respectively.

The degradation of the small-strain stiffness with shear strain is clearly observed in Figure 6(b) despite the small range of shear strains (G_v<0.5%) applied in RC tests. The normalized stiffness ($G_v/G_{v\text{-}max}$) was fitted using the hyperbolic relationship (Hardin and Drnevich 1972):

$$\frac{G_v}{G_{v\text{-}max}} = \frac{1}{\left(1+\frac{\gamma}{\gamma_{ref}}\right)} \quad (3)$$

where, γ_{ref} is a reference shear strain. Two main trends may be observed in Figure 6(b) which are represented by reference shear strains of 0.375 % (block) and 0.10 % (U75). Although the experimental data for specimen P100 seems to show a similar trend to the block sample up to γ=0.02%, the higher level of destructuration experienced by the P100 specimen (see following section) makes it plausible to expect quicker stiffness degradation at larger strain levels. The shear strain required to reduce the initial shear modulus to 0.70 G_v in the U75 specimen is about one order of magnitude lower (i.e., 0.033 %) than the block sample (0.21%). This shows the larger destructuration induced by the U75 Shelby tube.

4.3 Variation of soil damping with shear strain

The variation of the soil damping D with the shear strain is shown in Figure 6(c). For γ<0.005 %, D seems to increase linearly up to 3 %, irrespective of the sample provenance. It is apparent that at small strains, soil damping is not affected by the type of sampler, but different trends are observed at large shear strains. The U75 specimen reaches values up to 13.35 % whereas the value for the block sample remains lower than 4 %. It can be seen that D reduces after reaching a maximum value in the U75 specimen. Although no clear explanation has been found it is speculated here that this behaviour may be

due to modifications in the soil fabric caused by shear distortion on a partially disturbed clay sample. Further tests are required to confirm this hypothesis. The specimen P100 shows values closer to the block specimen for $\gamma<0.013$ % and then a deviation from this trend is observed. Ashmawy et al. (1995) observed minor influence of sampling disturbance on damping ratio at small strain but significant effects at large strain on reconstituted kaolinite slurry. The disturbed specimen appeared to have lower damping ratio curves, which is in disagreement with the results presented in this study. A possible reason for such discrepancy may be attributed to the fact that Ashmawy et al. induced sample disturbance by applying freezing-thawing cycles rather than tube sampling. On the other hand, laboratory results obtained by Safaqah and Riemer (2006), who employed two different tube samplers for inducing soil disturbance, showed good consistency with the behaviour presented in this paper. These results highlight the negative effect of some types of sampler on soil damping, an aspect that has been overlooked in previous studies despite its relevance for seismic design of geotechnical infrastructure. Further research is still needed in this field in order to obtain conclusive results.

Figure 6. Results from Resonant Column (RC) tests

4.4 Compressibility

The results of the CRS compression tests are presented in Figure 7. Vertical dashed lines are used in this figure to indicate the *in situ* vertical effective stress, $\sigma¢_{v\text{-}in\ situ}$, representative of the specimens. Figure 7(a) shows the variation of the volumetric strain with the vertical effective stress. Block and O89 specimens show the lowest volumetric deformation at $\sigma¢_{v\text{-in situ}}$ (less than 1.7 %) followed by the P100 and U75 specimens with 3.9 % and 12.5 %, respectively. The small deformation that has been required to reach $\sigma¢_{v\text{-in situ}}$ implies less degree of soil destructuration. This is consistent with the larger yield stress $\sigma¢_{yield}$ as well as the steeper slope of the compressibility curve post-yielding observed in block and O89 specimens, as shown in Figure 7(b). Grey stars are used in this figure to indicate the $\sigma¢_{yield}$, estimated using the Casagrande's graphical method as described in Holtz and Kovacs (1981). $\sigma¢_{yield}$ ranges from 65 kPa to 20 kPa. The value obtained from the U75 specimen, which is even lower than the $\sigma¢_{v\text{-in situ}}$ (i.e. OCR<1), is incompatible with the stress history of the marine deposits at the Ballina site. Specimen P100 shows a $\sigma¢_{yield}$ slightly higher than $\sigma¢_{v\text{-in situ}}$, thus, much lower than the level of overconsolidation ratio ($1.5 < OCR < 1.6$) reported by Pineda et al. (2016a).

Sampling disturbance is also reflected by the strong reduction in oedometric modulus, $M=d\sigma'_v/de$, observed in the overconsolidated range (see Figure 7(c)). The initial oedometric modulus reduces from 2.72 MPa (block sample) to 0.25 MPa (U75 sample). Block and the O89 specimens show a similar trend which is followed by the P100 specimen only at larger stress levels.

Figure 8 shows the variation of the compression index, $C_c=-¶e/¶\log(\sigma'_v)$, with the vertical effective stress normalized by the appropriate $\sigma¢_{yield}$ for each specimen in the normal compression range only. The strong non-linearity of C_c with $\sigma¢_v$ is characterized by a peak value, reached between 1.20 – 2.0 $\sigma¢_{yield}$. A constant value is reached at large stresses once the natural soil structure has been erased. As

expected, strong non-linearity is observed in the block and O89 specimens, with peak values of 2.95 and 2.25, respectively. Lower peak values of C_c are reported for P100 and U75 specimens (1.83 and 1.38, respectively) for which a more gentle post peak reduction in C_c is observed. The post peak value seems to be similar for all specimens tested (C_c » 1.30), except for the U75 sample (C_c » 1.0).

Figure 7. CRS compression test results

Figure 8. Variation of Cc with normalised stress level

Table 2 shows the estimated coefficient of consolidation, c_v, obtained from CRS tests according to ASTM D4186 (2006). Values reported in Table 2 show the $\sigma¢_{v\text{-}in\ situ}$ and $\sigma¢_{yield}$, as well as the value measured at $\sigma¢_v$ of 100 kPa. The c_v decreases substantially during one-dimensional compression and leads to a value around 0.20 m^2/year for an effective vertical stress around 100 kPa.

Table 2. c_v estimated from CRS tests.

4.5 Undrained shear strength

Figure 9 shows the temporal evolution of volumetric strain during the anisotropic consolidation stage at targeted K stress ratio in SS tests. Block and O89 specimens show a maximum volumetric strain around 2.5 %. This value is 2 and 3.3 times smaller than the deformation measured in P100 and U75 specimens, respectively.

The results of the undrained shearing stage are shown in Figure 10. Peak shear stresses, $\tau_{xy\text{-}peak}$, of 16.9 kPa, 16.7 kPa, 16.2 kPa and 14.6 kPa were measured in block, O89, U75 and P100 specimens, respectively. Despite the small variation in $\tau_{xy\text{-}peak}$ between specimens, attributed here to the lower void ratio achieved at the end of the consolidation stage (larger volumetric compression) for U75 and P100 specimens, important differences in the stress-strain response can be observed in Figure 10. A relatively brittle post-peak response, commonly displayed by structured soils, is shown by block and O89 specimens. Ductile behaviour is observed in P100 and U75 specimens. Values of shear strain at peak demonstrate the differences in stress-strain responses between block (3.87 %) and U75 (15.5 %) specimens. On the other hand, similar excess pore water pressure response is observed in Figure 10, at least up to about 5% shear strain. The increase in excess pore water pressure observed in the block specimen just after reaching $\tau_{xy\text{-}peak}$, appeared to be due to the propagation of a shear band.

The variation of the secant friction angle, ϕ'_{sec}, with the shear strain is presented in Figure 11. Two main trends are observed. Peak friction angles of 44° and 41° are observed in O89 and block specimens, respectively. At shear strains larger than 15 %, the friction angle reaches an average value of 36° for all

tested specimens as also reported by Pineda et al. (2016a). This value is similar to the critical state friction angle (constant volume conditions) reported by Mayne (2016) for a variety of natural soft soils such as Bothkennar clay (UK), Onsoy clay (Norway) and Burswood clay (Australia).

Figure 12 shows the variation of the secant shear modulus, $G_{u\text{-}sec}=\Delta\tau_{xy}/\Delta\gamma$, estimated from the stress-strain curves presented in Figure 10. Values around 3 MPa were measured for block, U75 and O89 specimens at shear strains around 0.02 %. At the same strain level, $G_{u\text{-}sec}$ reduces to 1.7 MPa for the P100 specimen. The U75 specimen shows lower values of shear secant modulus compared with block and O89 specimens. This does not reflect the strong difference in volumetric compression measured during consolidation, which suggest larger soil disturbance. In fact, it appears that soil destructuration caused by tube sampling using the Shelby tube is to some extent, at least in terms of soil stiffness, compensated by the large volumetric compression (densification) occurred during consolidation. More discernible differences in soil stiffness are observed between block and O89 specimens with respect to the P100. It might indicate that the stiffening effect produced by the reduction in void ratio during consolidation was smaller in this case than the destructuration caused by tube sampling.

Figure 9. Volumetric strain during K_0 consolidation

Figure 10. Results from the shearing stage in simple shear tests

Figure 11. Variation of the secant friction angle with the shear strain

Figure 12. Stiffness degradation curves

5 SAMPLING DISTURBANCE ASSESSMENT

The proposal by Lunne et al. (1997) has been adopted in this study to assess sample quality. This method is based on the change in void ratio required to recompress the soil to the *in situ* vertical effective stress in triaxial and CRS tests, normalized by the initial void ratio ($\Delta e/e_0$). For soils with OCR<2, Lunne et al. divide the sample quality into four levels as indicated in Table 3.

Table 3. Sample quality assessment according to Lunne et al. (1997) (OCR<2.0)

Figure 13 compares the sample quality descriptor ($\Delta e/e_0$) estimated for all tested specimens against the sampler diameter. It is clear that the block (Sherbrooke) and the fixed piston (O89) sampler consistently provide samples of *excellent* quality for all element testing. Extreme variation in sample quality, from *very poor* to *excellent*, is obtained from Shelby (U75) samplers, while the free piston sampler (P100) provides samples of *excellent* and *good to fair*.

Figure 13. Variation of the sample quality index with the sampler diameter

Figure 14 shows the variation of the shear wave velocities $Vs_{(vh)}$ and $Vs_{(hh)}$, measured in BE tests, against $\Delta e/e_0$. Shear wave velocities have been normalized against the value obtained from SDMT-8 test. As shown in Figure 5, $Vs_{(hh)}$ is less affected by sampling than $Vs_{(vh)}$, at least for unstressed conditions. Both $Vs_{(vh)}$ and $Vs_{(hh)}$ show values higher than 0.70 $Vs_{(in\ situ)}$. Once again, sample derived from block and O89 sampling show superior quality compared to other sampling techniques. A trend between the decrease in Vs with increasing $\Delta e/e_0$ may only be discerned for $Vs_{(hh)}$. However, further experimental data is required to get conclusive results.

Figure 14. Normalized shear wave velocities vs $\Delta e/e_0$

Figure 15, which shows the variation of modulus, G_v, and damping, D, as a function of $\Delta e/e_0$ measured in RC tests. Values of D plotted in this figure correspond to $\gamma = 0.05\%$. All tested specimens have *excellent* quality based on Lunne et al's. criterion, despite the important variation in G_v reported in this figure. G_v reduces in U75 and P100 specimens by about 45 % and 28 %, respectively, compared with the block ($G_{v(block)} \gg G_{(SDMT)}$). Values of D up to four times larger are clearly indicative of specimens with different quality. This potentially misleading relationship between the shear modulus and damping ratio measured in the RC device and $\Delta e/e_0$ may be attributed here to the stress path applied by the RC apparatus during consolidation. The isotropic recompression path followed in RC tests does not represent the true anisotropic stress state of the soil, due to the absence of the deviatoric component which contributes, to a large extent, to the deformation behaviour of the clay.

Figure 15. Variation of G_0 and D with $\Delta e/e_0$

Figure 16 compares the estimated σ'_{yield}, M and $C_{c\text{-}peak}$ against $\Delta e/e_0$ obtained from CRS tests. The trend shown in Figure 16 is qualitatively consistent with published data, i.e. the estimated σ'_{yield}, initial M and $C_{c\text{-}peak}$ decrease with reducing sample quality. $\sigma¢_{yield}$ reduces 30 % and 67 % in P100 and U75 specimens respectively. The reduction of M and $C_{c\text{-}peak}$ is even more dramatic. It may be noted that the P100 specimen has a *good to fair* quality according to the adopted sample quality criterion. This would imply that results from this specimen could be used with confidence in design, which would appear to be a misleading outcome judging by the comparison against mechanical properties measured in either block or O89 specimens.

The sample quality assessment for the specimens tested under simple shear conditions is shown in Figure 17. Peak undrained shear strength, $\tau_{xy\text{-}peak}$, shear strain at peak, γ_{peak}, as well as the undrained secant modulus at 50 % of $\tau_{xy\text{-}peak}$ are plotted against $\Delta e/e_0$. Despite the small variation of $\tau_{xy\text{-}peak}$ with

sample quality, the effects of sampling disturbance are clearer in terms of the stress-strain responses, which vary from brittle to ductile behaviour (see Figure 10). This is reflected in the value of shear strain measured at $t_{xy\text{-}peak}$ which increases up to 4 times that of the block sample in the U75 specimen. The P100 specimen classifies here as *good to fair* quality. This is a contradictory result based on the comparison of its mechanical response against block and O89 specimens.

Figure 16. Variation of σ'_{yield}, M and $C_{c\text{-}peak}$ with $\Delta e/e_0$

Figure 17. Variation of $\tau_{xy\text{-}peak}$,γ_{peak} and G_{u50} with $\Delta e/e_0$

6 IMPLICATIONS OF SAMPLING DISTURBANCE IN GEOTECHNICAL DESIGN

Although very good agreement between mechanical properties is shown for block and O89 specimens both of which had a sample quality index $\Delta e/e_0$ of 'excellent', misleading correlations are observed for specimens retrieved with free-piston (P100) and the Shelby (U75) samplers. This fact suggests some concerns about the reliability of soil parameters used in geotechnical design, where these samplers are used. As noted in the Introduction, fixed-piston samplers are not widely used in practice whereas the U75 Shelby sampler is the most common choice, especially in Australia.

Figure 18 compares values of yield stress (σ'_{yield}), compression index ($C_{c\text{-}peak}$), coefficient of consolidation (c_v at σ'_{yield}) and undrained shear strength (S_u) obtained for each sampler type against values obtained in the laboratory (Pineda et al. 2016a) and *in situ* (Kelly et al. 2017) characterization studies carried out at Ballina site. Laboratory tests reported by Pineda et al. (2016a), obtained from tube samples retrieved using the O89 sampler, provided specimens of 'excellent' and 'good' quality. Figure 18 reports values of coefficient of consolidation estimated from CRS tests, incremental loading (creep) tests as well as values of c_v obtained from CPTu tests. Undrained shear strength estimated from field vane (VT) tests, which provide similar values to those obtained from simple shear tests (e.g., Terzaghi et al. 1996; Kouretzis et al. 2017), are also reported in Figure 18 for comparison. Very good agreement is observed between laboratory values and *in situ* characterization studies and parameters estimated here for block and O89 samplers. This indicates that reliable predictions would be obtained by using soil parameters estimated from these samplers, particularly in the case of the block sampler. On the other hand, soil parameters estimated using P100 and U75 samplers are markedly lower compared to laboratory and *in situ* characterization studies (except for the undrained shear strength) which (a-priori) would lead to poor predictions.

Figure 18. Comparison between soil properties obtained in this study with parameters estimated from laboratory (Pineda et al. 2016a) and *in situ* (Kelly et al. 2017) characterization campaigns.

To assess the practical implications of sampling disturbance, two classical problems in soil mechanics are analysed in this paper, using the sets of soil parameters estimated in this study from each sampler type. To do so, the geometry of the trial embankment and the trial footing constructed at Ballina site by the

ARC Centre of Excellence for Geotechnical Science and Engineering (CGSE) were adopted here (see Figure 19). The embankment, constructed after installing vertical drains (PVDs) for accelerating soil consolidation, and the shallow footing were used in an International Prediction Symposium (CGSE, 2016) whose outcomes have been recently published by Kelly et al. (2018) and Doherty et al. (2018), respectively. With the aim of emphasizing the effects of sampling disturbance on predicted soil behaviour a few simplifications were made in the predictions presented below. Vertical drains were neglected whereas a single layer soil profile was adopted. Moreover, the original square footing was modelled as strip footing to use parameters from SS for plane strain condition. Although these assumptions made difficult a direct comparison between predicted and *in situ* measurements, the variation in predictions obtained using different samples can be compared with relevant field measurements.

Figure 19. (a) Embankment problem. (b) Footing problem

6.1 Settlement and excess pore pressure prediction underneath an embankment

The nominal dimensions of the embankment are (Figure 19(a)): 27 m long at the base, 15 m long at the crest, 3 m high and nominal inclination of 2H:1V. The total vertical surcharge applied by the embankment at the ground surface is 63 kPa. A simplified soil stratigraphy using one single layer (10.5 m in thickness) is adopted here for simplicity. No prefabricated vertical drains are considered in this exercise.

Predictions of settlement as well as excess pore pressure underneath the centreline of the embankment were made using the four sets of parameters obtained from CRS tests (1 per sampler type) summarized in Table 4. The following predictions were made (see also Appendix 1):

- End of primary consolidation settlement due to the weight of the embankment using 1-D consolidation theory (Equations A1 and A2 in Appendix 1).
- Time variation of excess pore water pressure, degree of consolidation and consolidation settlement due to the construction of the embankment via the Finite Difference Method (FDM) (Equations A3 to A5 in Appendix 1).

Based on the value of $\sigma¢_{yield}$ obtained from the block specimen, which experienced lower disturbance during sampling and therefore should represent more closely the *in situ* conditions, the entire soil profile moved from overconsolidated (OC) to normally consolidated (NC) conditions at the end of construction of the embankment (σ'_{final} = 105 kPa). However, it will take some time for each soil layer to reach equilibrium in effective stresses due to the consolidation experienced by the clay. This is particularly important for the selection of c_v to be used in the prediction because it reduces substantially once yielding occurs. Values of c_v reported in Table 4 correspond to the average between $\sigma'_{v\text{-in situ}}$ and σ'_{yield} (OC states) and the average between σ'_{yield} and $\sigma'_{100\ kPa}$ (NC states).

Table 4: Parameters obtained from CRS tests used in settlement and excess pore pressure predictions underneath an embankment

Figure 20 compares the predicted surface settlements using the set of compressibility parameters determined from CRS tests for each sampler type. Larger total settlement is predicted when using parameters obtained from block or O89 specimens which had sample quality indexes of 'excellent'. The settlement curve predicted for the P100 specimen is similar to those obtained for the block and O89. Although this result would be considered in agreement with its sample quality index of 'good to fair', it may be noted the important differences in soil properties between this sample and block and O89 specimens shown in Figures 7 and 8. Total settlement is mainly controlled by σ'_{yield} and C_c. The 'good' settlement prediction obtained for the P100 specimen is attributed here to the counterbalance effects of a lower compression index (that reduced the predicted total settlement) and a lower yield stress (that increased the predicted total settlement). Figure 20 also shows the underestimation of total settlement when soil parameters are obtained using disturbed specimens such as those obtained with the U75 sampler. The predicted total settlement after 1000 days is 0.76 m, 0.80 m and 0.84 m when using block,O89 and P100 soil parameters, respectively. The predicted total settlement reduces to 0.32 m if parameters from U75 specimens are adopted, which equates to an apparent reduction in total settlement of 60 % with respect to the predicted value using block parameters, is thus observed. In this case, the reduction in Cc had more effect on the predicted total settlement than the reduction in σ'_{yield}. Underestimation of total settlement caused by embankment construction on soft clay has been commonly observed in Australian practice. This result is likely, to a large extent, due to the use of inappropriate sampling techniques, such as the U75 Shelby tube.

Predicted excess pore water pressures are shown in Figure 21. Two trends are observed. Similar excess pore pressure dissipation is predicted using parameters from block and O89 specimens. The slower excess pore pressure dissipation predicted using parameters derived from P100 and U75 specimens may be explained by the important reduction in c_v post-yielding which is more dramatic in specimens previously subjected to large sample disturbance (P100 and U75). After 2000 days, the dissipation of excess pore water pressure was still higher than 90%. This is the reason why no secondary compression settlement has been considered into settlement curves presented in Figure 20.

Figure 20. Predicted embankment surface settlement

Figure 21. Predicted pore pressure dissipation curves at depth of 6 m

6.2 Settlement and bearing capacity of a strip footing

Figure 19(b) shows the geometry of the shallow footing, which is modified from the square footing built at the Ballina field testing facility (Gaone et al. 2018) to a strip footing. The strip footing has a width of 2.0 m and 0.6 m in height. The footing base is located at 1.4 m below the ground surface. Predicted settlement and undrained bearing capacity were calculated using the parameters obtained from simple shear (SS) tests summarized in Table 5. It includes values of undrained shear strength and secant modulus determined at 50 % of the peak shear strength. The values were obtained from Figure 12 using the shear

strain at which $\tau_{xy}=\tau_{xy\text{-}peak}/2$.

Table 5: Parameters obtained from SS tests

The footing elastic settlement was calculated using Equation A6 (see Appendix 2) which considered the foundation embedment depth and the location of rigid layers at limited depth. The undrained bearing capacity was computed according to Prandtl's solution (Equation A7 in Appendix 2) including shape, depth and inclination correction factors.

Figure 22 compares the predicted undrained bearing capacity, q_f, and the elastic settlement, s_e at q_f. Similar q_f values (135 - 140 kPa) were obtained using parameters from block, O89 and U75 specimens. Despite the quite different stress-strain response observed in SS tests (Figure 10), the reduction in q_f is less than 11 %, a value that seems within the acceptable range of uncertainty in most geotechnical problems. s_e varies from 77 mm to 123 mm, with largest values predicted with the parameters from the P100 specimen. The results presented above indicate that, despite the different stress-strain responses observed in SS tests, prediction of undrained bearing capacity of shallow footing in Ballina clay is not strongly affected by sampling disturbance but certainly affect the determination of the elastic settlement. Differences of more than 60 % are observed when comparing settlement due to block and P100 samples, for example.

Figure 22. Predicted bearing capacity against predicted settlement for the footing problem

7 CONCLUDING REMARKS

Safe and cost-effective geotechnical design is critically dependent on the representativeness of soil parameters, as these affect the accuracy of the associated predictions. An evaluation of the effects of sampling disturbance caused by different sampling tools on soil parameters estimated from laboratory tests and their consequences in geotechnical design has been presented in this paper. Sample quality assessment has confirmed that, as previously reported for other natural soft soils worldwide, block samples as well as fixed-piston samples provide specimens of excellent quality. On the other hand, misleading sample properties are obtained for specimens retrieved with free-piston samplers and Shelby tubes, when their mechanical properties are compared with block specimens.

The implications of sampling disturbance in geotechnical design were highlighted using predictions made for an embankment as well as a shallow footing problem. Total settlement prediction underneath an embankment is strongly affected by sampling disturbance as a consequence of the important reduction in $\sigma¢_{yield}$ and compression index. Practitioners have to be aware of the fact that there are cases where correct predictions can be achieved, but for the wrong reasons, which by no means reflects good practice. It may occur, for instance, when the reduction in C_c is largely compensated for by the reduction in

$\sigma\phi_{yield}$.

On the other hand, despite the differences in stress-strain behaviour observed in undrained simple shear tests, the predicted undrained bearing capacity seems to be less influenced by sampling disturbance despite the important discrepancies in stress-strain behaviour observed in undrained tests. From a practical perspective, it is important to remark that reliable and cost-effective predictions of geotechnical infrastructure is possible with minimum improvements to the current practice for sampling and testing of soft clays, in particular, by incorporating fixed-piston samplers into current practice.

ACKNOWLEDGEMENT

The research presented here forms part of the activities of the Centre for Offshore Foundation Systems (COFS), currently supported as a node of the Australian Research Council Centre of Excellence for Geotechnical Science and Engineering (CGSE) (grant CE110001009). The authors are grateful for support by all contributing partners to the CGSE. These partners include Fugro AG, Coffey Geotechnics and Douglas Partners, and the NSW Science Leveraging Fund of NSW.

REFERENCES

Ashmawy, A.K.; Salgado, R.; Guha, S.; and Drnevich, V.P. 1995. Soil Damping and Its Use in Dynamic Analyses. *International Conferences on Recent Advances in Geotechnical Earthquake Engineering and Soil Dynamics*, 35-41, St. Louis, Missouri.

Andersen A., Kolstad P. 1979. The NGI 54-mm samplers for undisturbed sampling of clays and representative sampling of coarser materials. In: Proc. Int. Symp. Soil Sampling, Singapore, pp 13–21.

ASTM D4186-06 2006. *Standard test method for one-dimensional consolidation properties of saturated cohesive soils using controlled-strain loading*, vol. 10, ASTM International.

ASTM D4015 2007. *Standard Test Methods for Modulus and Damping of Soils by Resonant-Column Method*. ASTM International.

ASTM Standard D6528 2007, *Standard Test Method for Consolidated Undrained Direct Simple Shear Testing of Cohesive Soils*, ASTM International.

Clayton, C.R.I. 2011. Stiffness at small strain research and practice. *Geotechnique*, 61(1), 5-37.

Clayton, C.R.I., Simmons N.E., and Matthews, M.C. 1995. Site investigation. 3rd Ed., University of Surrey, London, United Kingdom.

CGSE (Australian Research Council Centre of Excellence for Geotechnical Science and Engineering). 2016. http://CGSE.edu.au (accessed 10/006/2017)

Christian, J.T., and Carrier III, W.D. 1978. Janbu, Bjerrum and Kjaernsli's chart reinterpreted. *Canadian Geotechnical Journal*, *15*(1), 123-128.

Doherty, J. Gourvenec, S., Gaone, F., Pineda, J.A., Kelly, R., O'Loughlin, C.D., Cassidy, M.J., and Sloan, S.W. 2018. A novel web based application for storing, managing and sharing geotechnical data, illustrated using the National Soft Soil Field Testing Facility in Ballina, Australia. *Computers and Geotechnics,* 93, 3-8.

Donohue S., and Long, M. 2010. Assessment of sample quality in soft clay using shear wave velocity and suction measurements. Geotechnique, 60(11), 883-889.

Gaone, F., Doherty, J., and Gouvernec, S. 2018. Large-scale shallow foundation load tests on soft clay - at the National Field Testing Facility (NFTF), Ballina, NSW, Australia. *Computers and Geotechnics, 93, 253-268*.

Hardin, B.O.,and Drnevich, V.P. 1972. Shear modulus and damping in soils: design equations and curves. *Journal of Soil Mechanics & Foundations Div*, 98(7), 667-692.

Hight, D.W., Bond, A.J., and Ledge, J.D. 1992. Characterization of the Bothkennar clay: an overview. *Géotechnique*, 42(2), 303-347.

Holtz, R.D., and Kovacs, W.D. 1981. An Introduction to Geotechnical Engineering. Prentice-Hall, Inc., New Jersey, 733 pp.
Janbu, N., Bjerrum, L., and Kjaernsli, B. 1956. "Veiledning vedlosning av fundamentering—soppgaver," *Publication No. 18,* Norwegian Geotechnical Institute, pp. 30–32.

Kelly, R.B., Pineda, J.A., Bates, L., Suwal, L., and Fitzallen, I. 2017. Site characterisation for the Ballina field testing facility. *Géotechnique*, 67(4), 279-300.

Kelly, R.B., Sloan, S.W., Pineda, J.A., Kouretzis, G., and Huang, J. 2018. Outcomes of the Newcastle Symposium for the prediction of embankment behaviour on soft soil. *Computers an*d Geotechnics, 93, 9-41.

Kouretzis, G., Pineda, J.A., Krabbenhoft, K., and Wilson, L. 2017. Interpretation of vane shear tests for geotechnical stability calculations. Canadian Geotechnical Journal, 54(12), 1775-1780.

Lacasse, S., Berre, T., and Lefebvre, G. 1985. Block sampling of sensitive clays. Proceedings, 11th International Conference on Soil Mechanics and Foundations Engineering (2), San Francisco: 887-892.

Ladd, C.C., and DeGroot, D.J. 2003. Recommended practice for soft ground site characterization: Arthur Casagrande Lecture. In Proc. 12th PanAmerican Conference on Soil Mechanics and Geotechnical Engineering (eds P.J. Culligan, H.H. Einstein and A.J. Whittle), vol 1, 3-57. Esses, Germany: Verlag Gluckauf GmbH.

Landon M., DeGroot D., and Sheanan, T.C. 2007. Nondestructive sample quality assessment of a soft clay using shear wave velocity. J. Geotechnical and Geoenvironmental Engineering, 133(4), 424-432.

Lefebvre, G., and Poulin, C. 1979. A new method of sampling in sensitive clay. *Canadian Geotechnical Journal*, 16(1), 226-233.

Lunne, T., Berre, T., Andersen, K., Strandvick, S., and Sjursen, M. 2006. Effects of sample disturbance and consolidation procedures on measured shear strength of soft marine Norwegian clays. *Canadian Geotechnical Journal*, 43(7), 726-750.

Lunne, T., Berre, T. and Strandvick, S. 1997. Sample disturbance effects in soft low plastic Norwegian clay. In Proc. *Symposium on Recent Developments in Soil and Pavement Mechanics*, Rio de Janeiro, Brazil (ed. M. Almeida), 81–92. Rotterdam, the Netherlands: Balkema.

Mao, X., and Fahey, M. 2003. Behaviour of calcareous soils in undrained cyclic simple shear. *Geotechnique*, 53(8), 715-727.

Mayne, P.W., and Poulos, H.G. 1999. Approximate displacement influence factors for elastic shallow

foundations. *Journal of Geotechnical and Geoenvironmental Engineering*, 125(6), 453-460.

Mayne, P.W. 2016. Evaluating effective stress parameters and undrained shear strength of soft-firm clays from CPTu and DMT. In Proc. 5th International Conference on Geotechnical and Geophysical Site Characterization, ISC5, Gold Coast, Queensland, Australia, (eds: Lehane, Acosta-Martinez and Kelly), Australian Geomechanics Society Press, 19–40.

Mesri, G., and Choi, Y. 1985. Settlement analysis of embankments on soft clays. *Journal of Geotechnical Engineering*, 111(4), 441-464.

Pineda, J.A.,Suwal, L.P., Kelly, R.B., Bates, L., and Sloan, S.W. 2016a. Characterisation of Ballina clay. *Géotechnique*, 66(7), 556-577.

Pineda, J.A., Liu, X-F., and Sloan S.W. 2016b. Effects of tube sampling in soft clay: a microstructral insight. *Geotechnique*, 66(12), 969-983.

Safaqah, O.A., and Riemer, M.F. 2006. Minimizing sampling disturbance using a new in situ device. *Soil Dynamics and Earthquake Engineering*, *26*(2), 153-161.

Tanaka, H., Sharma, P., Tsuchida T., and Tanaka, M. 1996. Comparative study on sample quality using several types of samplers. *Soils and foundations*, 36(2), 57-68.

Terzaghi K., Peck R.B., and Mesri G. 1996. Soil mechanics in engineering practice. John Wiley & Sons.

Viggiani, G., and Atkinson, J.H. 1995. Interpretation of bender element tests. *Géotechnique*, 45(1), 149-154.

Figure Captions

Figure 1. Variation of index properties with depth at the Ballina field testing facility (modified from Pineda et al. 2016a)

Figure 2. Location of the boreholes at the Ballina field testing facility

Figure 3. Samplers used in this study. (a) Shelby tube (from Clayton et al. 1995). (b) Free piston sampler. (c) Fixed-piston sampler (from ASTM D6519-08). (d) Sherbrooke (block) sampler.

Figure 4: Specimen allocation in a tube (U75, P100 and O89 tube specimens) and block samples.

Figure 5. Variation of (a) shear wave velocity and (b) normalised shear wave velocity with sampler diameter

Figure 6. Results from Resonant Column (RC) tests

Figure 7. CRS compression test results

Figure 8. Variation of Cc with normalised stress level

Figure 9. Volumetric strain during K_0 consolidation

Figure 10. Results from the shearing stage in simple shear tests

Figure 11. Variation of the secant friction angle with the shear strain

Figure 12. Stiffness degradation curves

Figure 13. Variation of the sample quality index with the sampler diameter

Figure 14. Normalized shear wave velocities vs $\Delta e/e_0$

Figure 15. Variation of G_0 and D with $\Delta e/e_0$

Figure 16. Variation of σ'_{yield}, M and $C_{c\text{-}peak}$ with $\Delta e/e_0$

Figure 17. Variation of $\tau_{xy\text{-}peak}$, γ_{peak} and G_{u50} with $\Delta e/e_0$

Figure 18. Comparison between soil properties obtained in this study with parameters estimated from laboratory (Pineda et al. 2016a) and *in situ* (Kelly et al. 2017) characterization campaigns.

Figure 19. (a) Embankment problem. (b) Footing problem

Figure 20. Predicted embankment surface settlement

Figure 21. Predicted pore pressure dissipation curves at depth of 6 m

Figure 22. Predicted bearing capacity against predicted settlement for the footing problem

Table 1: Dimensions of the samplers used in this study

Sampler	Type	Length, L	Outer diameter, D_e	Thickness, t	Outer cutting angle, OCA	D_e/t	Area ratio, AR
	(-)	mm	mm	mm	degrees	-	(%)
U75	Open sampler	600	76	1.5	15	50.7	8.4
P100	Free piston	600	100	3.0	90	33.3	13.2
O89	Fixed piston	700	89	2.0	5	46.8	9.6
Sherbrooke	Block sampler	350	250	-	-	-	-

Table 2. c_v estimated from CRS tests.

Vertical stress parameter (kPa)	c_v (m^2/year)			
	Block	P100	O89	U75
$\sigma¢_{v\text{-in situ}}$	2.7	3.0	6.0	0.28
$\sigma¢_{yield}$	1.7	1.5	3.0	0.7
$\sigma¢_{v,\ 100\ kPa}$	0.17	0.2	0.7	0.2

Table 3. Sample quality assessment according to Lunne et al. (1997) (OCR<2.0)

Quality	**De/e_0**
Very good to excellent	< 0.04
Good to fair	0.04 – 0.07
Poor	0.07– 0.14
Very poor	>0.14

Table 4: Parameters obtained from CRS tests used in settlement and excess pore pressure predictions underneath an embankment

Sampler	σ'_{yield}	Compression index, C_c	Swelling index, C_s	c_v,	
				before yield	after yield
	(kPa)	(-)	(-)	(m^2/yr)	(m^2/yr)
Block	65	2.94	0.23	2.20	0.95
P100	45	1.83	0.24	2.25	0.85
O90	62	2.21	0.20	4.5	1.85
U75	42	1.29	0.17	0.50	0.2

Table 5: Parameters obtained from SS tests

Sample	Secant Modulus at 50 % strength, G_{50}	Undrained shear strength, s_u
	(kPa)	(kPa)
Block	1260	16.89
P100	710	14.64
O90	990.5	16.64

U75	1100	16.2

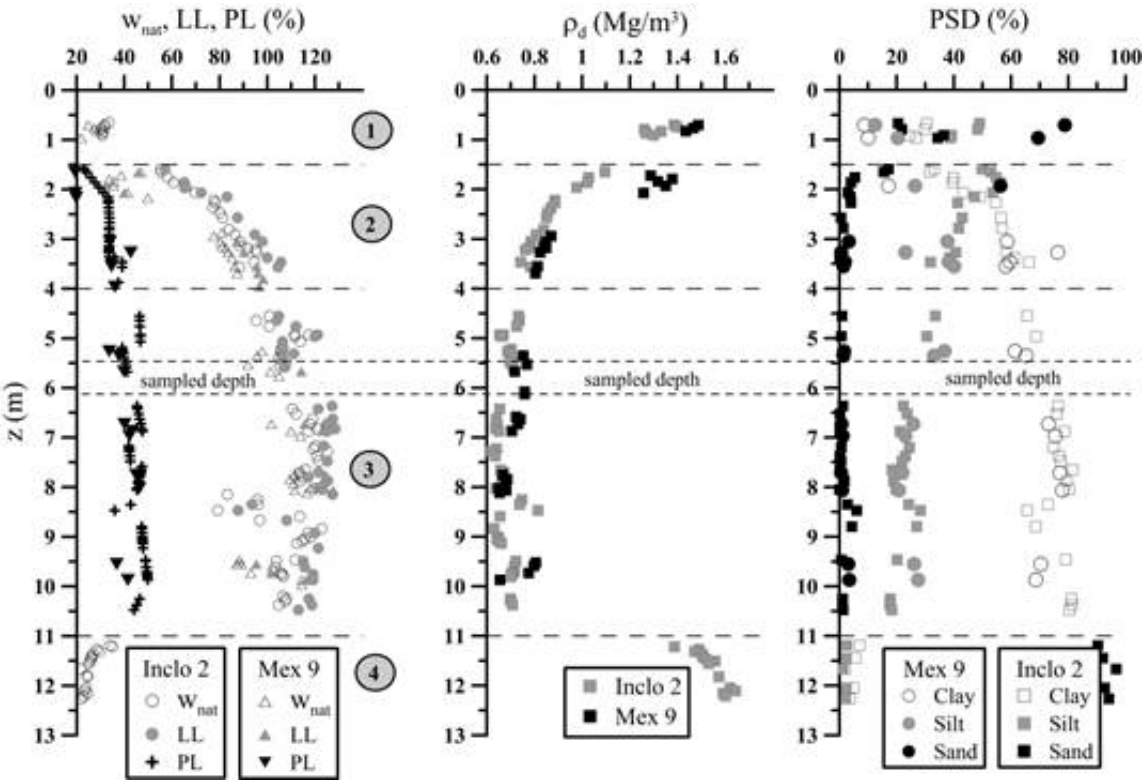

Figure 1.

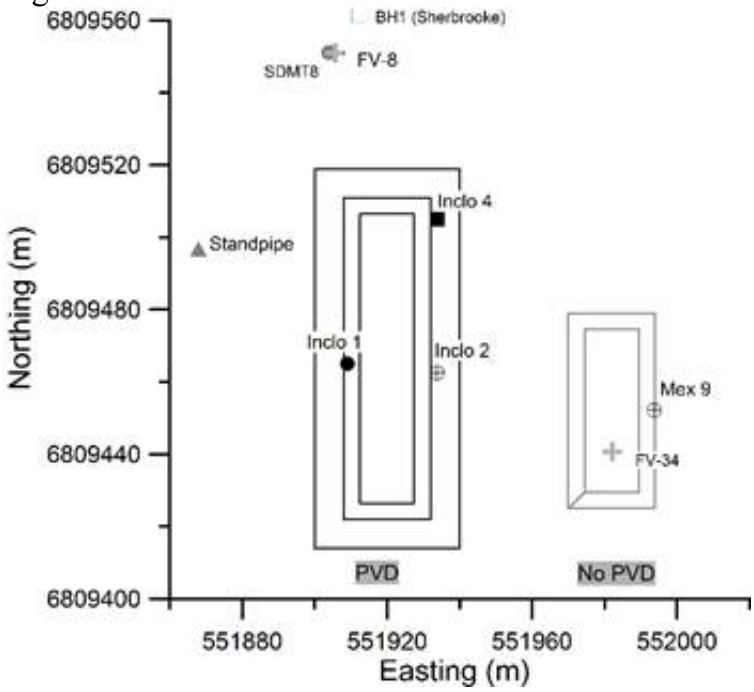

Figure 2.

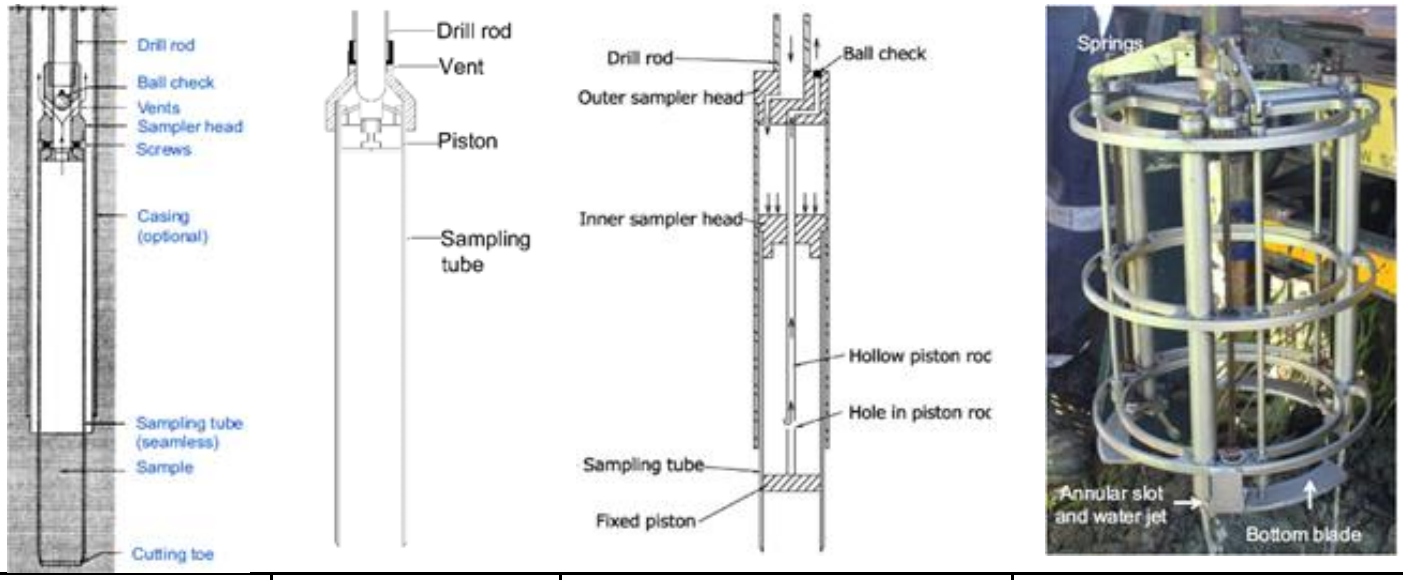

(a)	(b)	(c)	(d)

Figure 3.

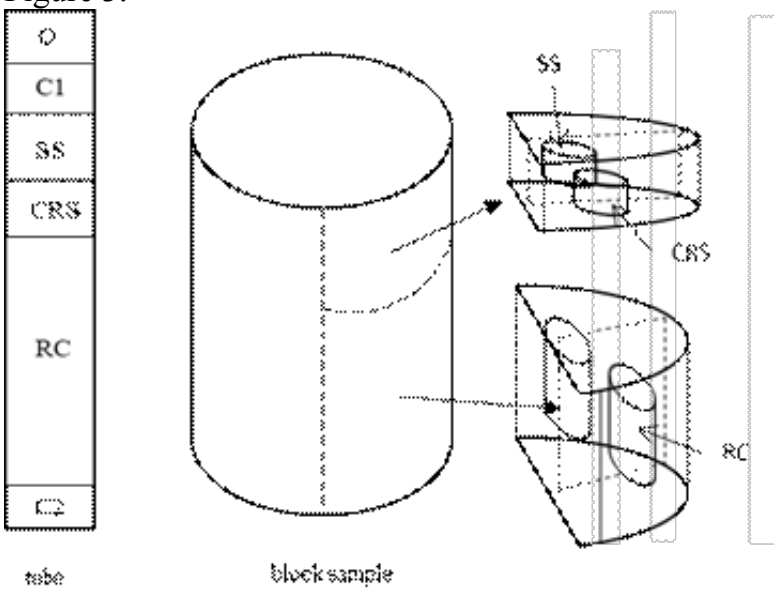

Figure 4.

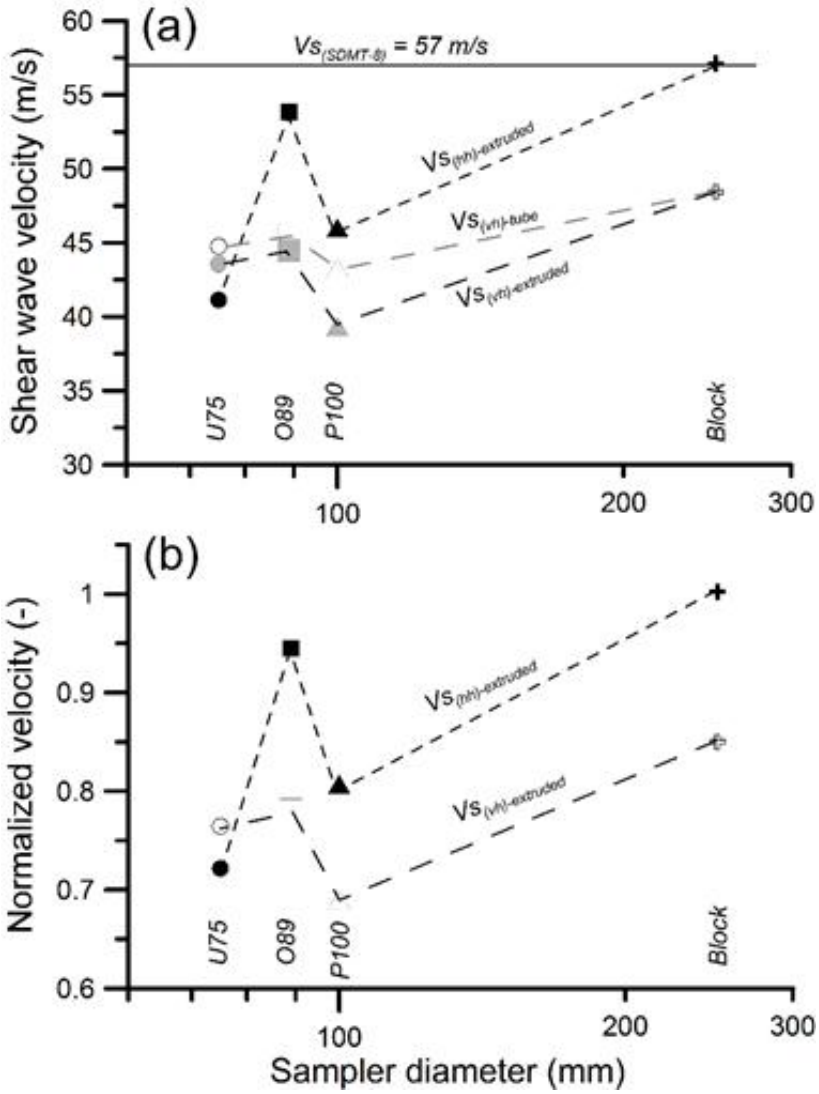
(a)
Vs(SDMT-8) = 57 m/s
Vs(hh)-extruded
Vs(vh)-tube
Vs(vh)-extruded
Shear wave velocity (m/s)
60
55
50
45
40
35
30
U75
O89
P100
Block
100
200
300
(b)
Vs(hh)-extruded
Vs(vh)-extruded
Normalized velocity (-)
1
0.9
0.8
0.7
0.6
U75
O89
P100
Block
100
200
300
Sampler diameter (mm)

Figure 5.

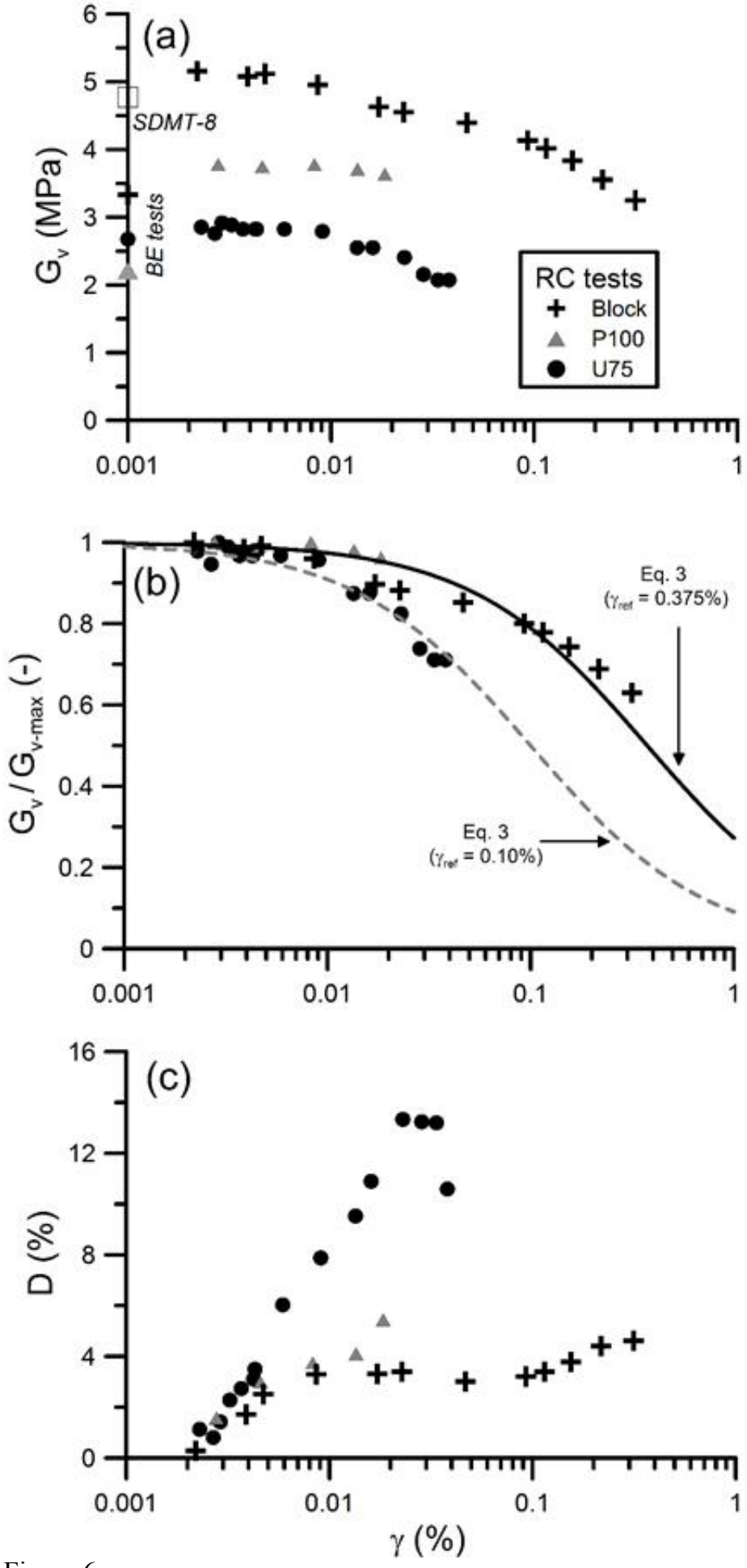
(a)
SDMT-8
BE tests
RC tests
Block
P100
U75
G_v (MPa)
(b)
Eq. 3
(γ_{ref} = 0.375%)
Eq. 3
(γ_{ref} = 0.10%)
$G_v / G_{v\text{-}max}$ (-)
(c)
D (%)
γ (%)

Figure 6.

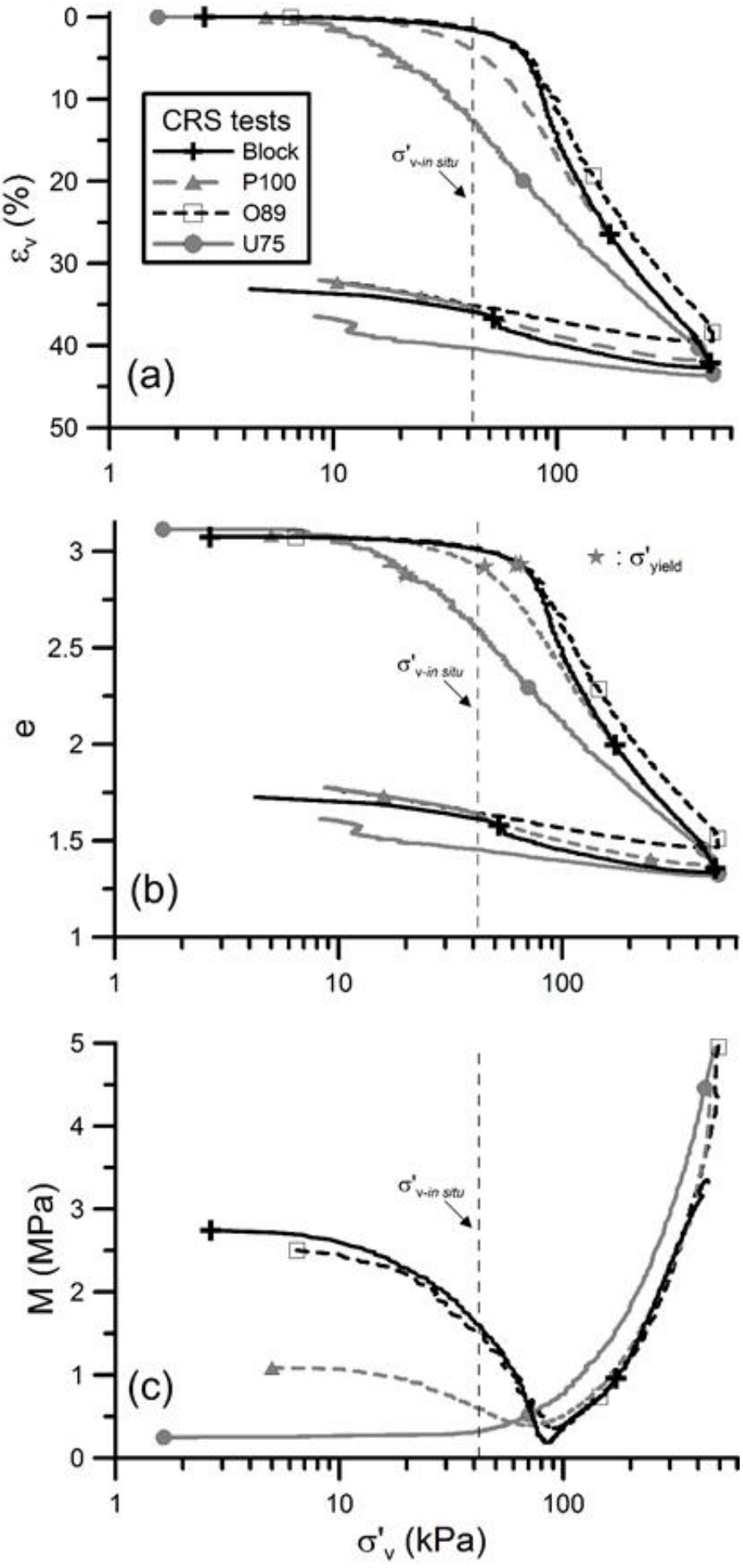
CRS tests
Block
P100
O89
U75
σ'v-in situ
(a)
εv (%)
0
10
20
30
40
50
1
10
100
★ : σ'yield
σ'v-in situ
(b)
e
3
2.5
2
1.5
1
σ'v-in situ
(c)
M (MPa)
5
4
3
2
1
0
σ'v (kPa)

Figure 7.

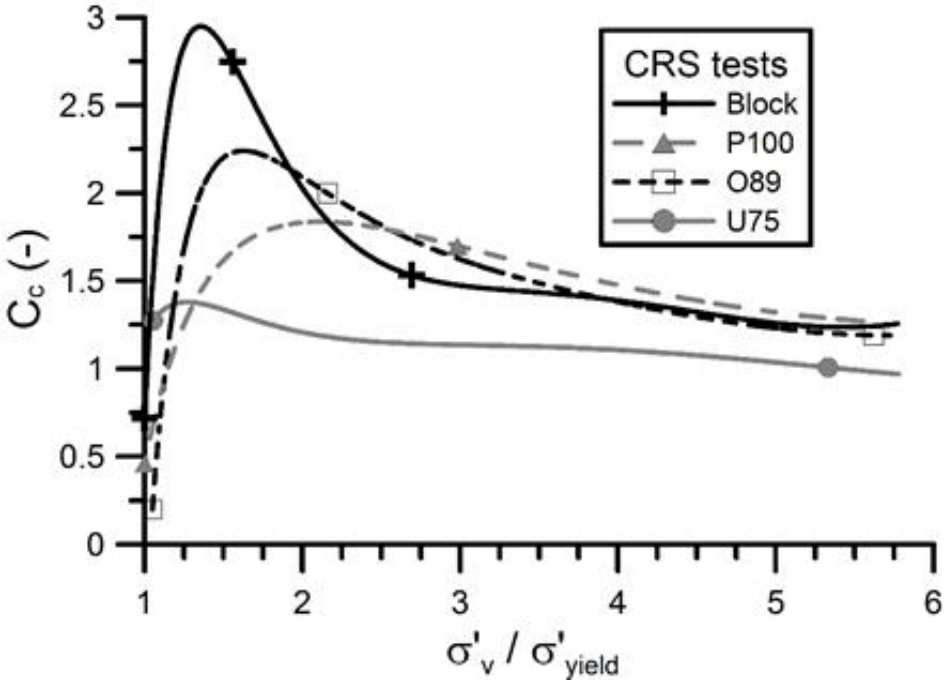

Figure 8.

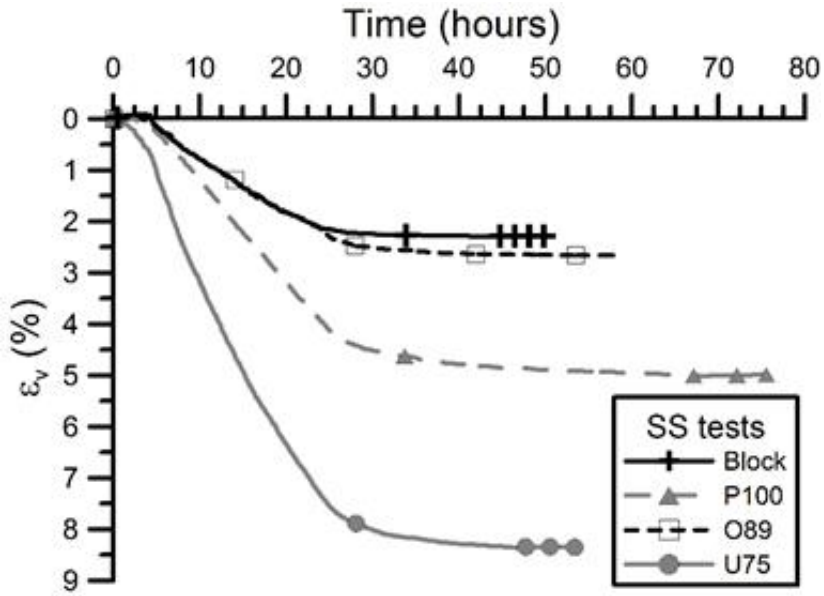

Figure 9.

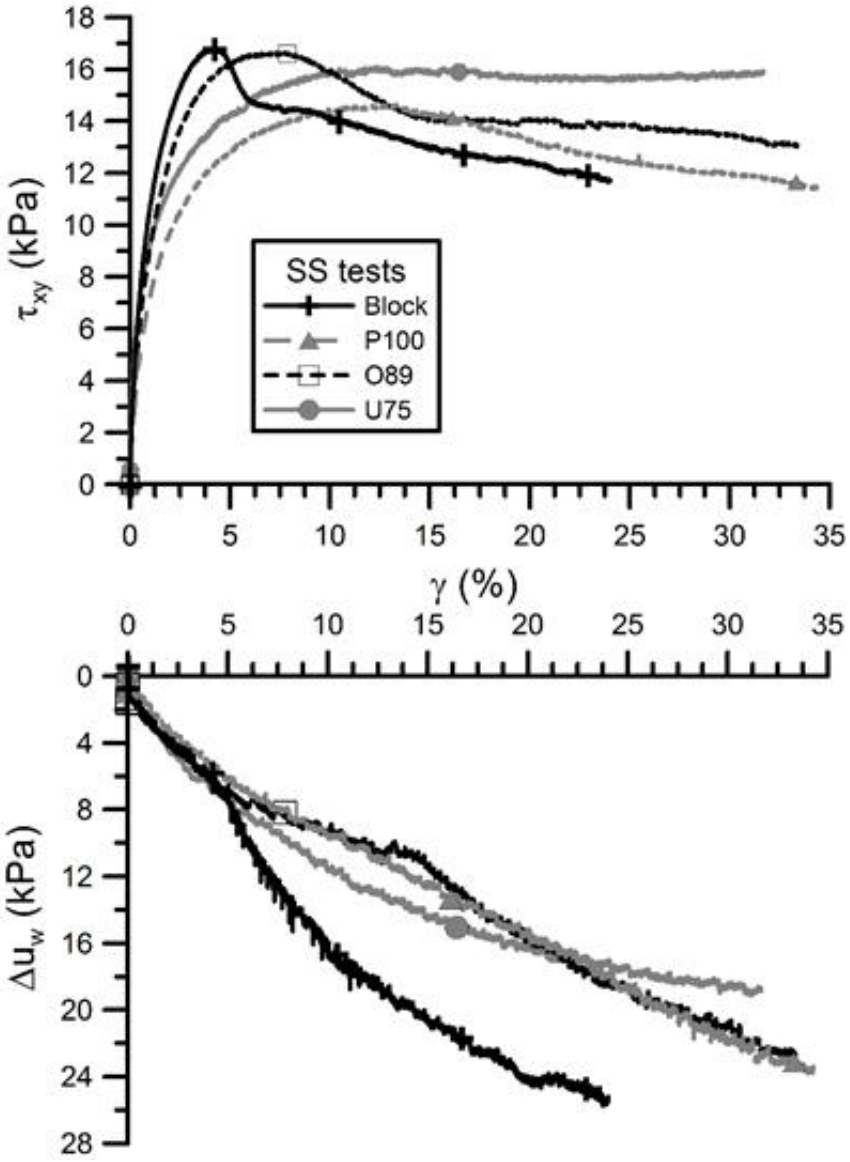

Figure 10.

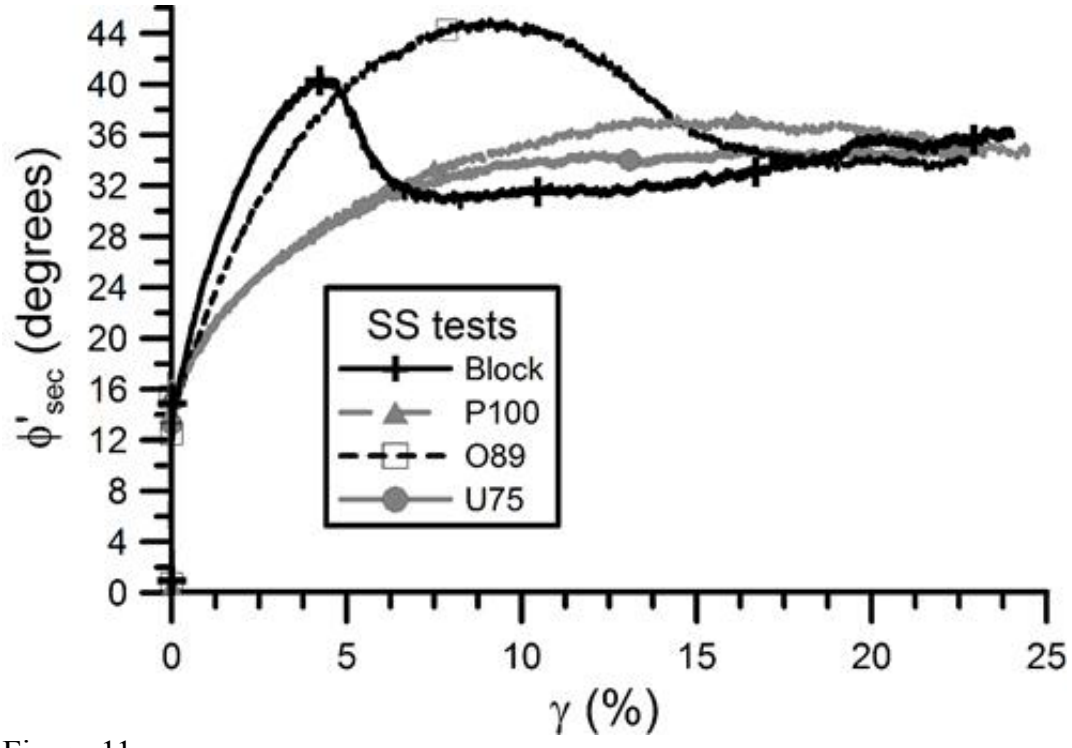

Figure 11.

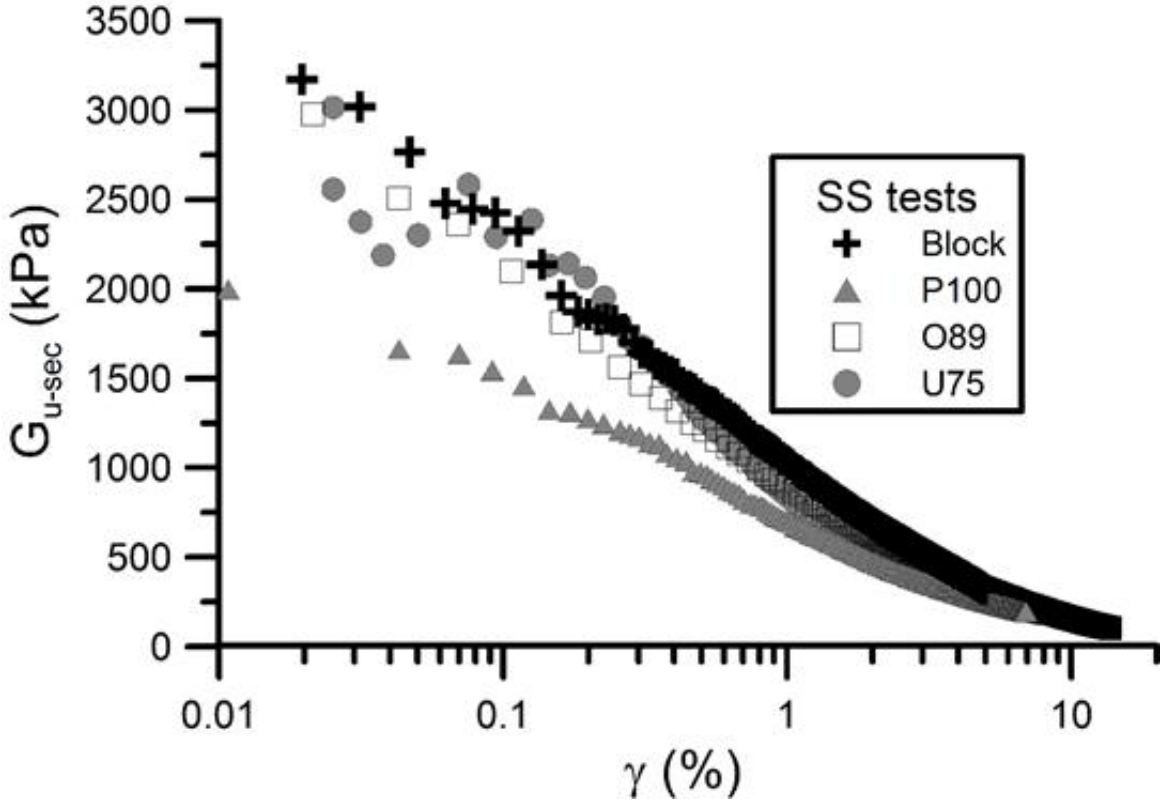

Figure 12.

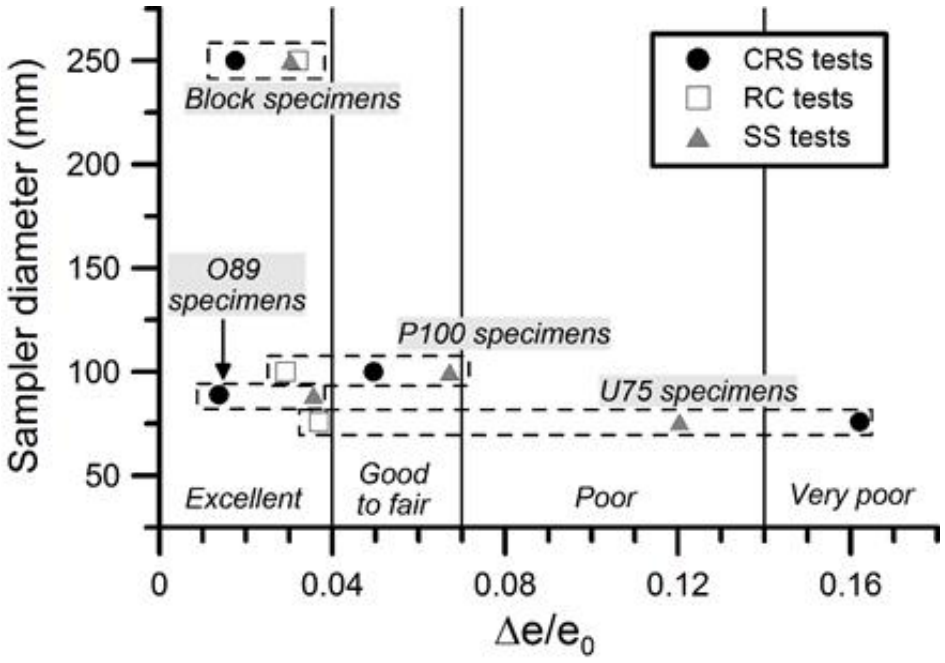

Figure 13.

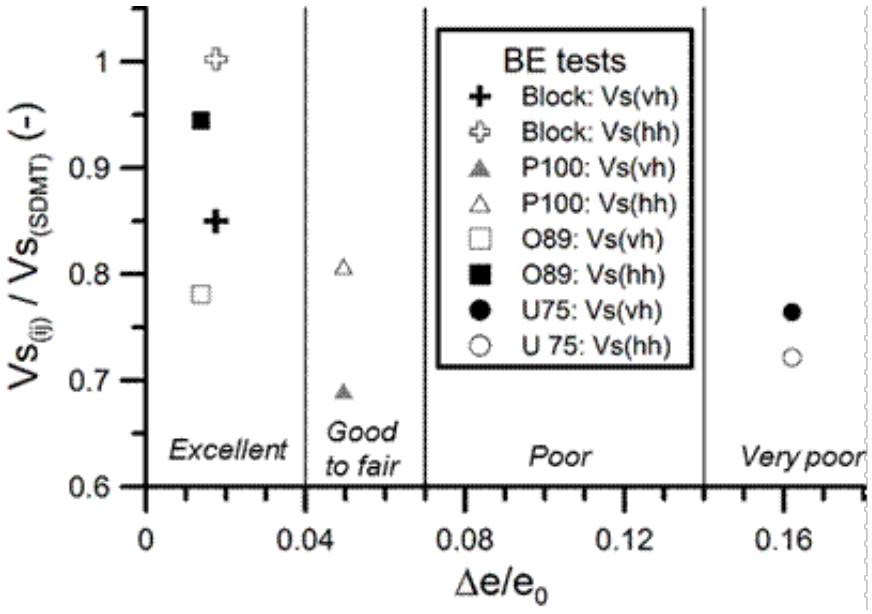

Figure 14.

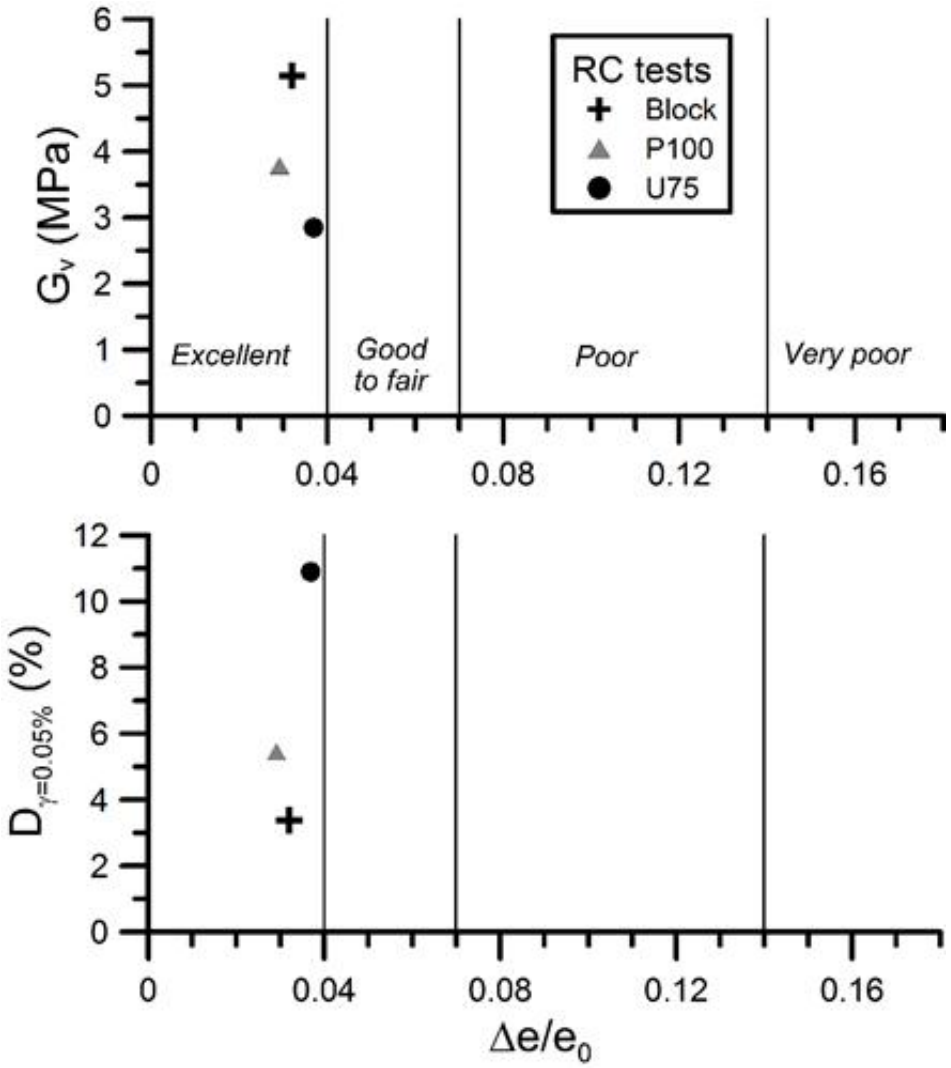

Figure 15.

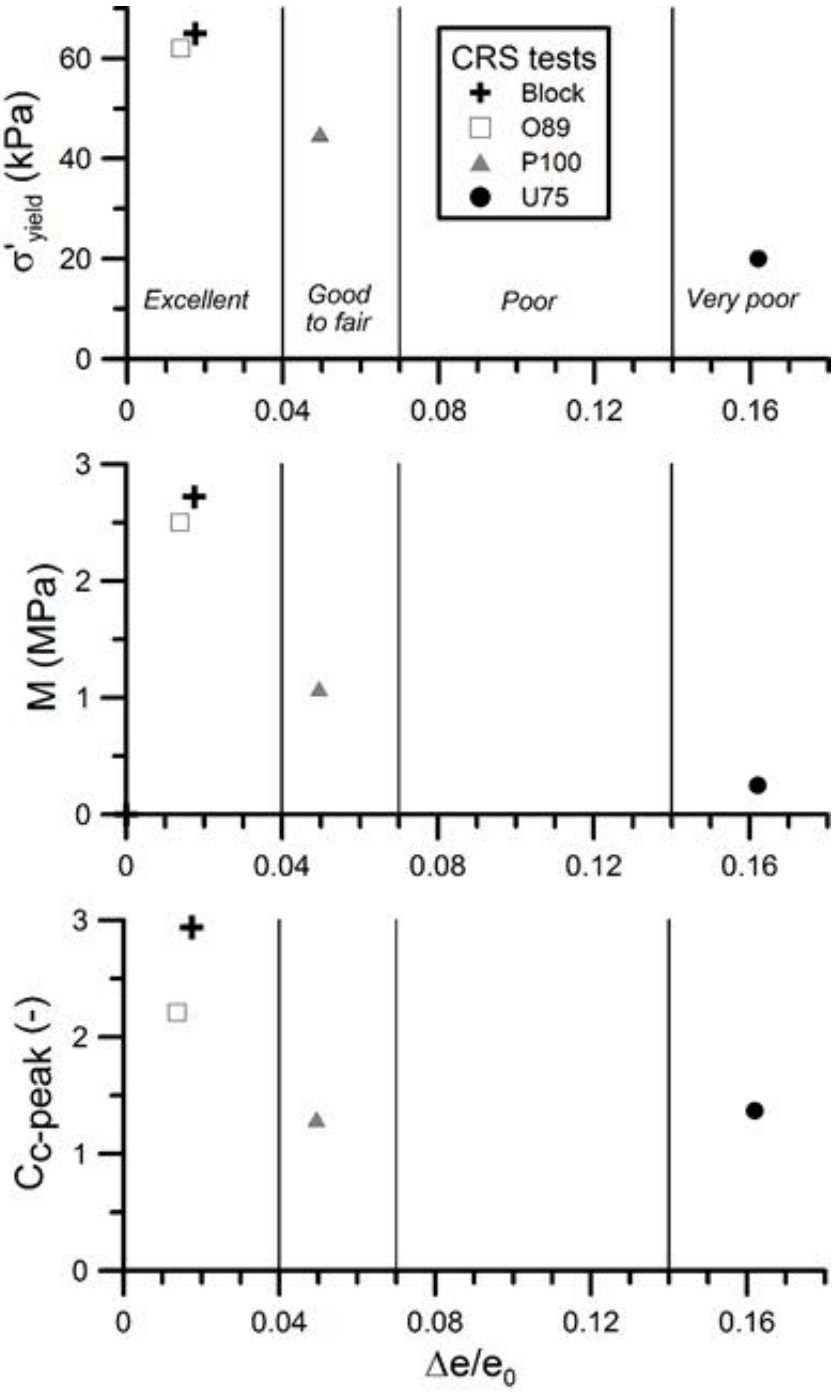
CRS tests
Block
O89
P100
U75
σ'yield (kPa)
Excellent
Good to fair
Poor
Very poor
M (MPa)
Cc-peak (-)
Δe/e0
0
0.04
0.08
0.12
0.16
20
40
60
1
2
3

Figure 16.

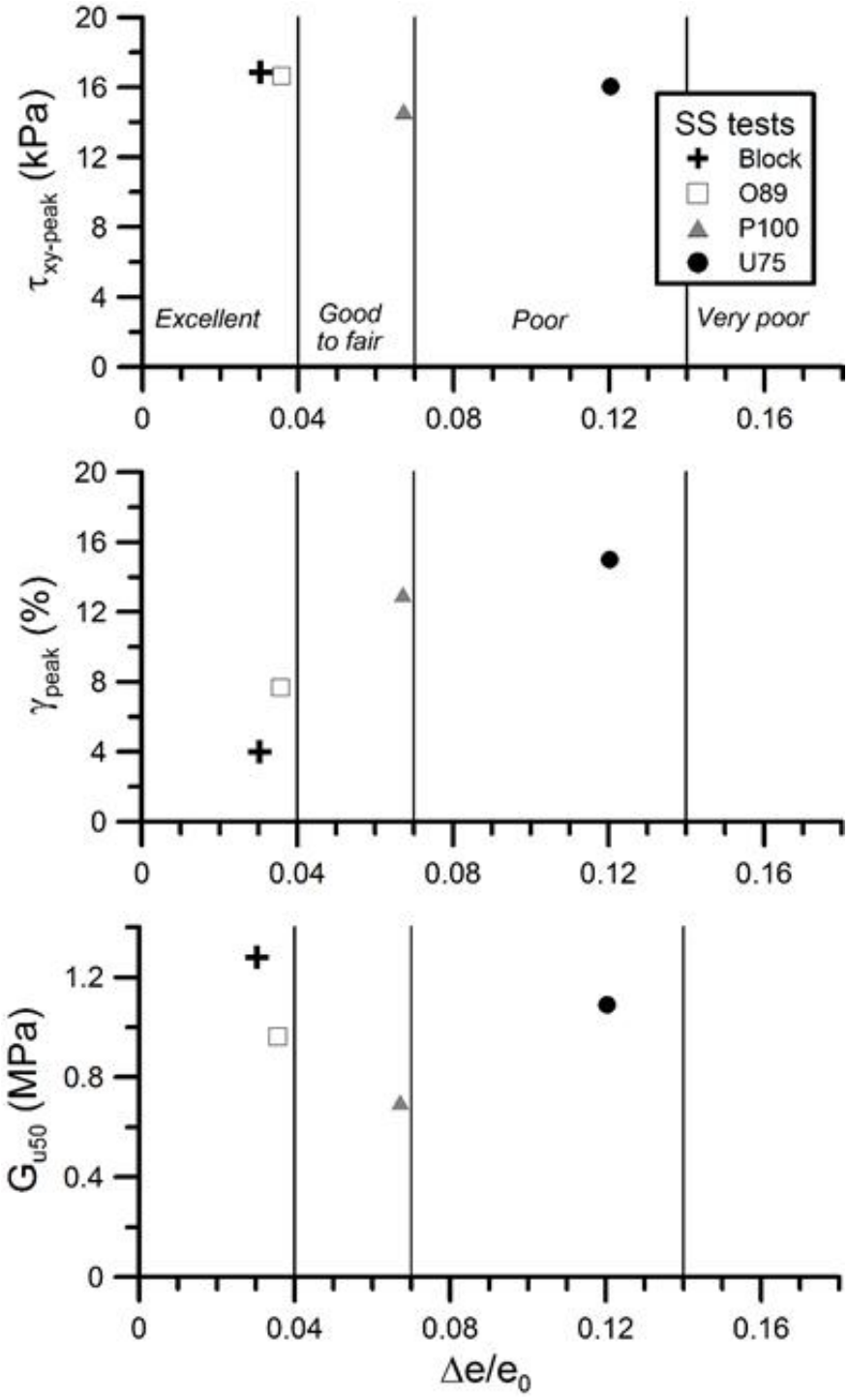
20
16
12
8
4
0
$\tau_{xy\text{-}peak}$ (kPa)
SS tests
Block
O89
P100
U75
Excellent
Good to fair
Poor
Very poor
0
0.04
0.08
0.12
0.16
γ_{peak} (%)
1.2
0.8
0.4
G_{u50} (MPa)
$\Delta e/e_0$

Figure 17.

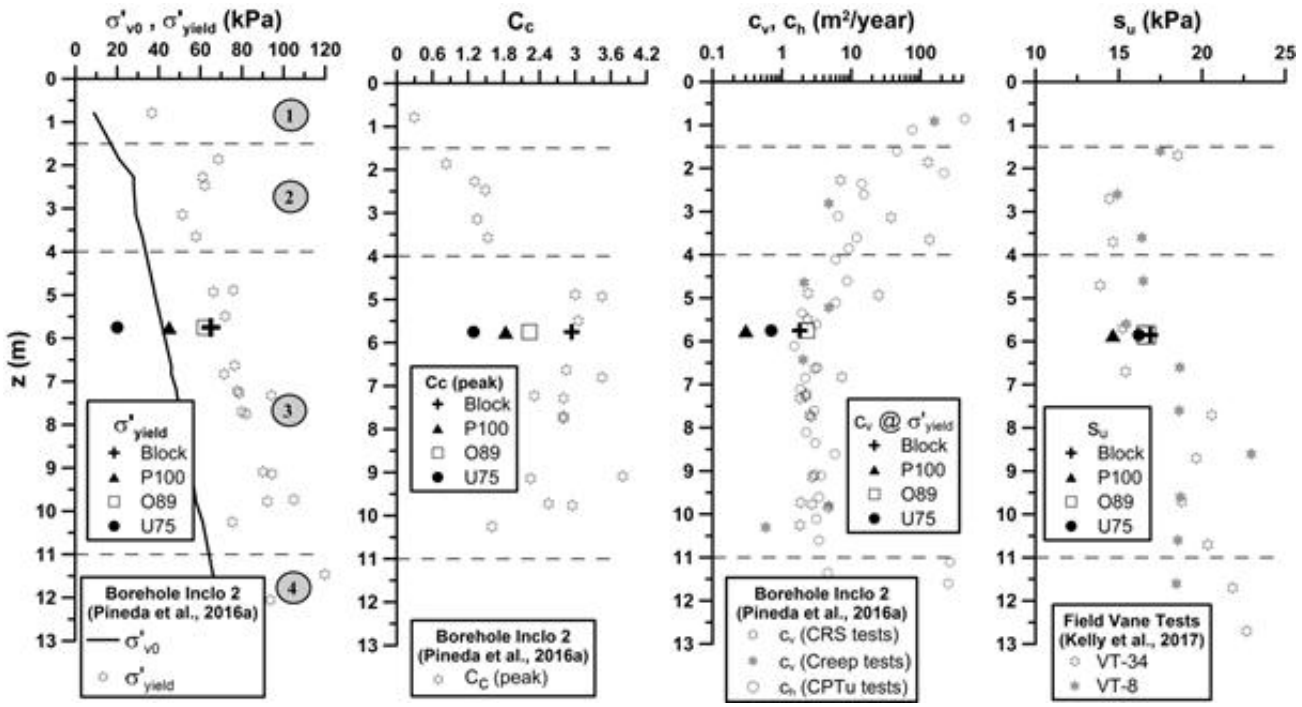

Figure 18.

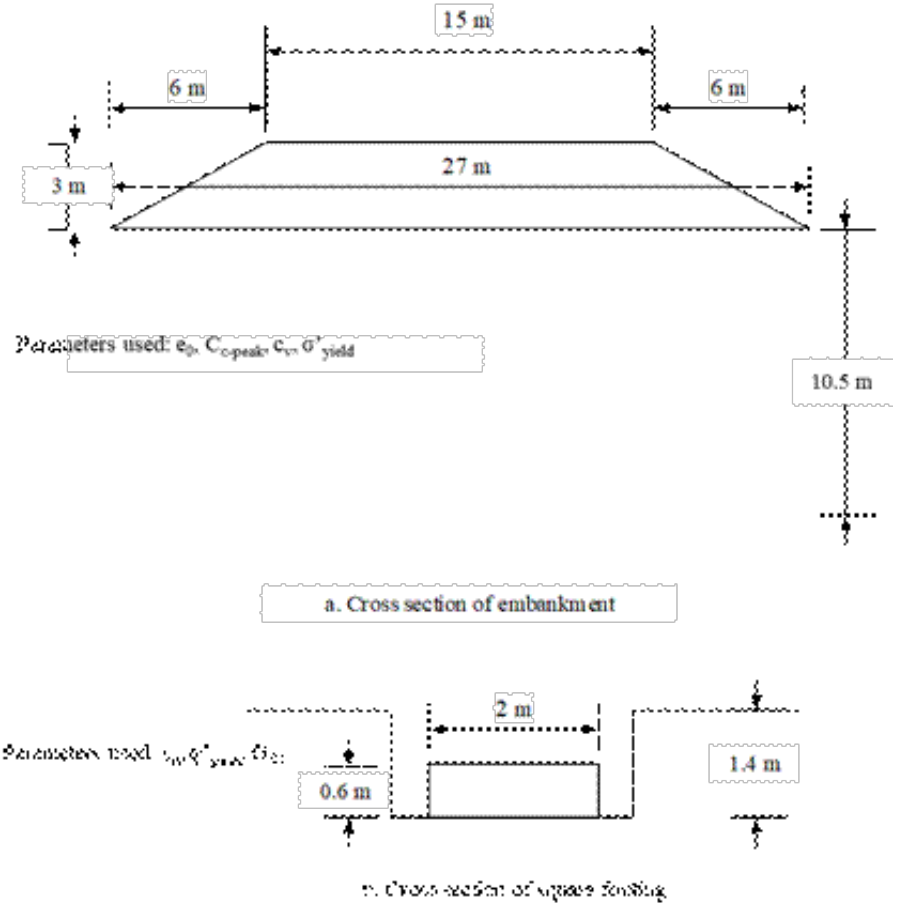

Figure 19.

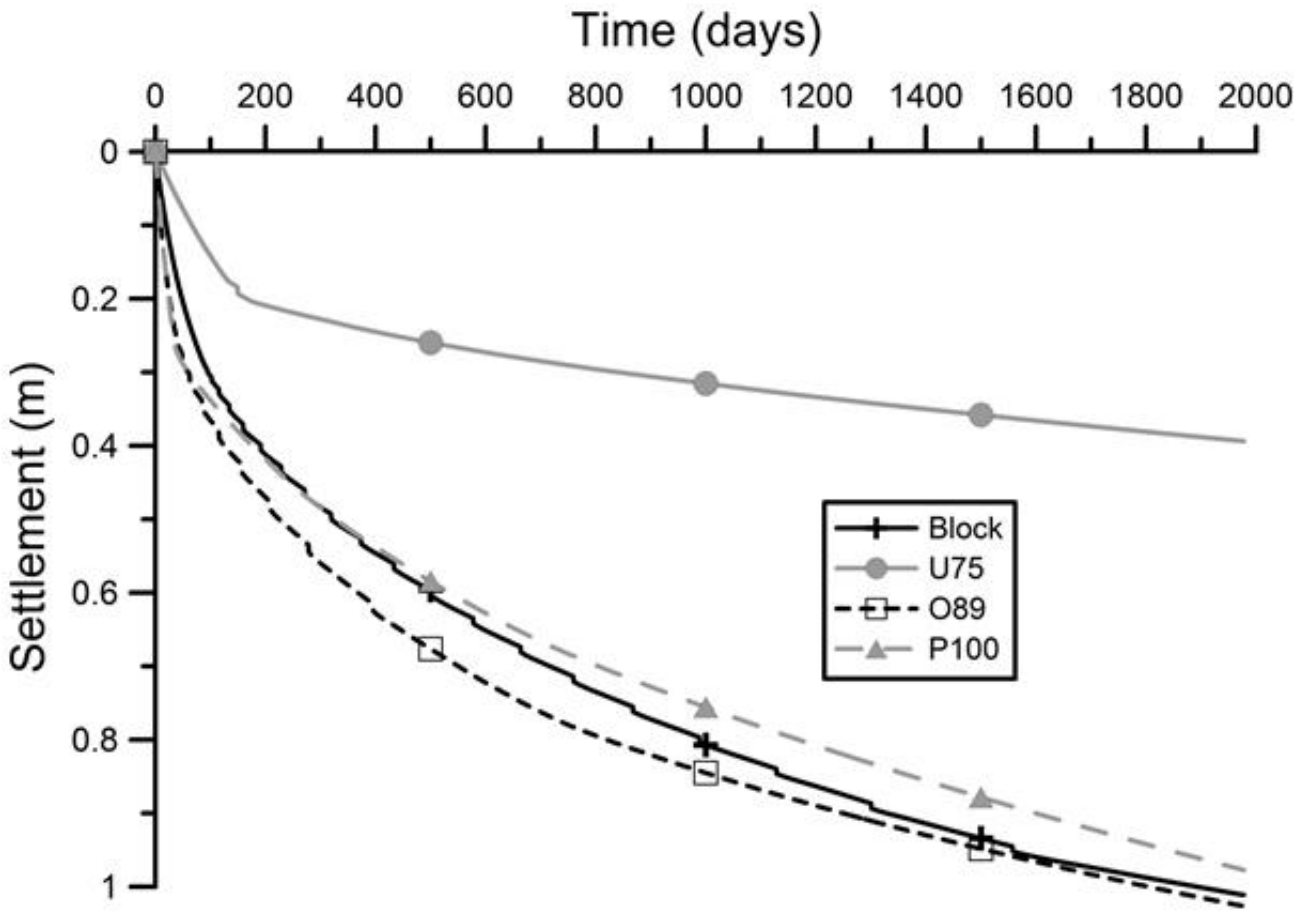

Figure 20.

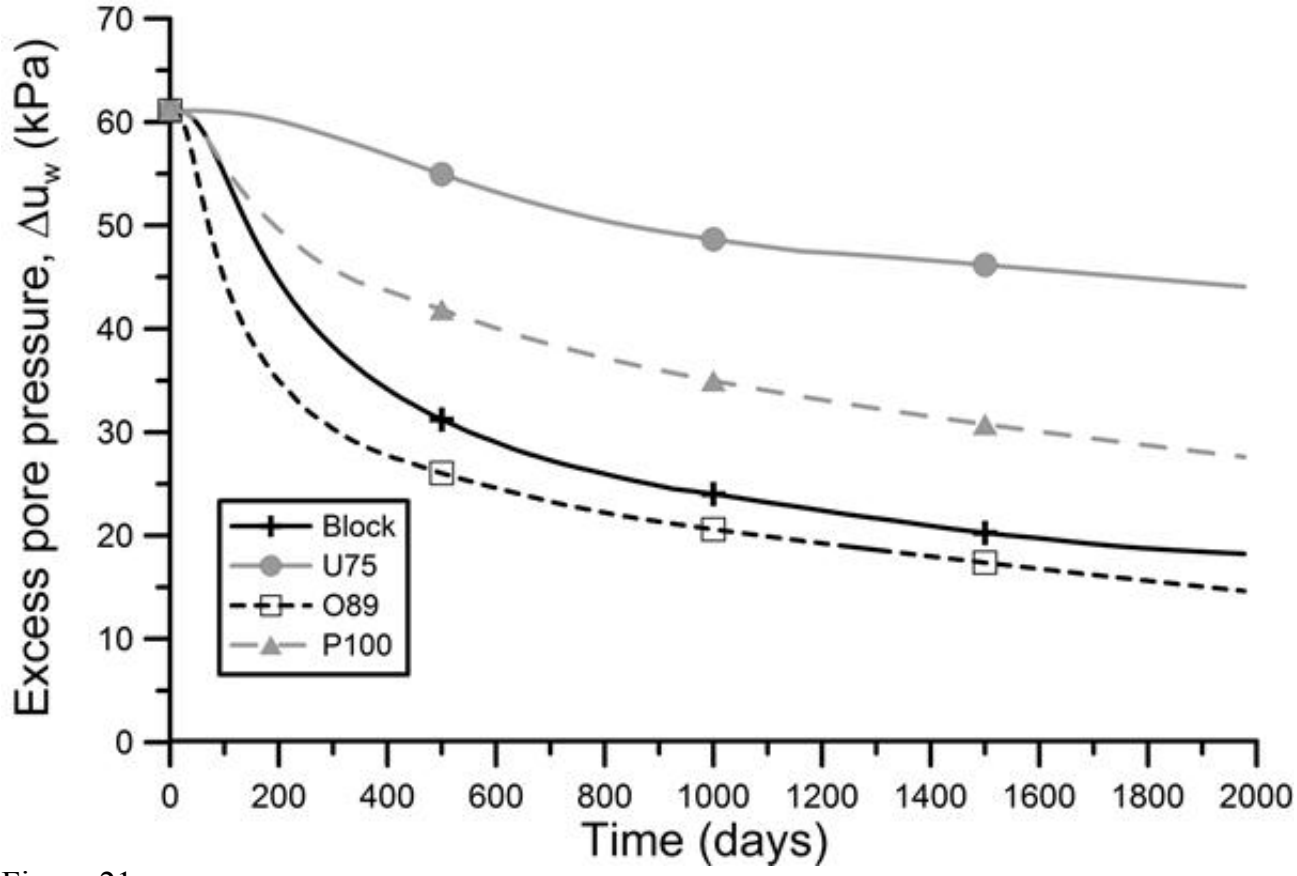

Figure 21.

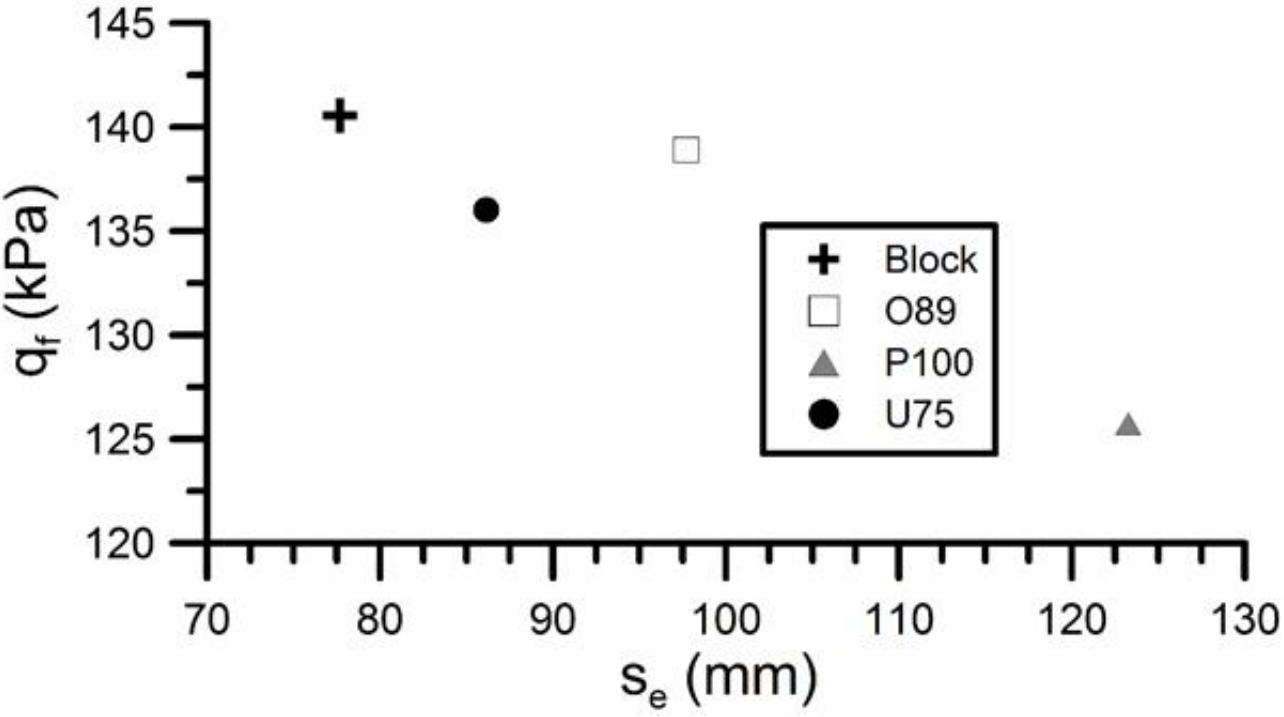
145
140
135
130
125
120
q_f (kPa)
70
80
90
100
110
120
130
s_e (mm)
Block
O89
P100
U75

Figure 22.

APPENDIX 1: CALCULATION OF SETTLEMENT AND EXCESS PORE WATER PRESSURE DUE TO THE EMBANKMENT CONSTRUCTION

The primary consolidation settlement was determined from 1-D consolidation theory using either Equations A1 or A2, depending on the current stress state of the soil (OC or NC). Equation A1 was used in cases where the final effective stress was less than the $s¢_{yield}$ ($s_{final\text{-}OC}$). If the current stress state reached values larger than the $s¢_{yield}$, Equation A2 was employed for stress increments beyond this value ($s_{final\text{-}NC}$).

$$s_{final\text{-}OC} = \frac{C_r}{1+e_0} h_z \log\left[\frac{\sigma'_{initial}+\Delta\sigma_z}{\sigma'_{initial}}\right] \quad (A1)$$

$$s_{final\text{-}NC} = \frac{C_r}{1+e_0} h_z \log\left[\frac{\sigma'_{yield}}{\sigma'_{initial}}\right] + \frac{C_c}{1+e_0} h_z \log\left[\frac{\sigma'_{initial}+\Delta\sigma_z}{\sigma'_{yield}}\right] \quad (A2)$$

where s_{final} is the settlement of the layer, e_0 is the initial void ratio, C_c is the compression index, C_r is the recompression index, h_z is the height of the layer, $s'_{initial}$ is the initial vertical effective stress and s'_{yield} is the yield stress.

FDM was used here to compute the dissipation of excess pore pressure due to consolidation (Equation A3) as it allows the variation in soil parameters (e.g., the consolidation coefficient c_v) with nodes due to its fundamental algorithm. The degrees of consolidation as well as the settlement s_t, at any time t, were calculated using Equations A3 to A5:

$$u(i, j+1) = u(i,j) + \beta\left[u(i-1, j) + u(i+1, j) - 2u(i,j)\right] \quad \text{where } \beta = \frac{c_v t}{h_z^2} \quad (A3)$$

$$U = \left[\frac{u_0 - u_{(i,j)}}{u_0}\right] \quad (A4)$$

$$s_t = U \times s_{final} \quad (A5)$$

where s_{final} is the final settlement, U is the average degree of consolidation, u_0 is the initial excess pore pressure, $u_{(i,j)}$ is the excess pore pressure at node i at time j and c_v is the coefficient of consolidation.

Appendix 2: Calculation of settlement and bearing capacity of a shallow footing

The average settlement of a flexible footing on saturated clay soil with given Poisson's ratio of soil, n as 0.5 was computed as follows:

$$s_e = \mu_1 \mu_2 \frac{q_0 B}{E_0} \quad (A6)$$

where μ_1 is the correction factor for finite thickness of an elastic soil layer, μ_2 is the correction factor for

depth of embedment of foundation, q_0 is the net applied pressure on the foundation, B is the width of the strip footing, and E_0 is elastic soil modulus. The details of the correction factors can be found in Christian and Carrier (1978) who modified the original correction factors by Janbu et al. 1956.

The undrained bearing capacity was calculated as follows:

$$q_f = 5.14\, s_c\, d_c i_c s_u \quad \text{(A7)}$$

where s_c is shape correction factor, d_c is depth correction factor, i_c is simplified Meyerhof inclination factor and s_u is the undrained shear strength. Correction factors were estimated as follows:

$s_c = 1 + 0.2\left(\frac{B}{L}\right)$; B = width and L = length of footing

$d_c = 1 + 0.4\left(\frac{D}{B}\right)$ if (D/B) ≤ 1

$d_c = 1 + 0.4\, tan^{-1}\left(\frac{D}{B}\right)$ if (D/B) > 1 where D =depth of footing